

Modeling and Analysis of Hormone and Mitogenic Signal Integration in Prostate Cancer

Katharine V. Rogers, Joseph A. Wayman, Ryan Tasseff, Caitlin Gee, Matthew P. DeLisa, and Jeffrey D. Varner*

School of Chemical and Biomolecular Engineering
Cornell University, Ithaca NY 14853

Running Title: Modeling signal transduction in prostate cancer

To be submitted: *Molecular Systems Biology*

*Corresponding author:

Jeffrey D. Varner,

Associate Professor, School of Chemical and Biomolecular Engineering,
244 Olin Hall, Cornell University, Ithaca NY, 14853

Email: jdvarner@cornell.edu

Phone: (607) 255 - 4258

Fax: (607) 255 - 9166

Abstract

Prostate cancer is the most common cancer in men and the second leading cause of cancer related death in the United States. Androgens, such as testosterone, are required for prostate cancer growth. Androgen ablation in combination with radiation or chemotherapy remains the primary non-surgical treatment for androgen dependent prostate cancer. However, androgen ablation typically fails to permanently arrest cancer progression, often resulting in castration resistant prostate cancer (CRPC). CRPC is closely related to metastasis and decreased survival. In this study, we developed and analyzed a population of mathematical models describing growth factor and hormone signal integration in androgen dependent, intermediate and resistant prostate cancer cells. The model describes the integration of two simultaneous extracellular signaling inputs, namely, androgen and growth factors into a G1/S cell cycle checkpoint decision. Model parameters were identified from 43 studies in androgen dependent and resistant LNCaP cell lines. The model was validated by comparing simulations with an additional 29 data sets from LNCaP cell lines that were not used during training. Additionally, data from four drug trials was also used to evaluate the model's performance. Sensitivity analysis, conducted over an ensemble of prostate signaling models, suggested that in an androgen free environment general translation and transcription was more sensitive in androgen dependent cells, while in androgen independent cells the PI3K and MAPK pathway species were more sensitive. In a constant DHT environment sensitive species were conserved between the cell lines. These results suggest targeting the PI3K and MAPK pathways in addition to anti-androgen therapies as a treatment for CRPC.

Keywords: Prostate cancer, signal transduction, mathematical modeling

1 Introduction

2 Prostate cancer (PCa) is the most commonly diagnosed cancer and the second leading
3 cause of cancer-related death in men in the United States [82]. Initially, PCa cells depend
4 upon the activation of cytosolic androgen receptors (AR) by androgen hormones, such
5 as testosterone, for survival and growth. Androgen ablation in combination with radiation
6 or chemotherapy remains the primary non-surgical treatment for androgen dependent
7 prostate cancer (ADPC) [43]. However, androgen ablation typically fails to permanently
8 arrest cancer progression as malfunctioning cells eventually lose androgen sensitivity and
9 proliferate without hormone. The loss of androgen sensitivity results in castration resistant
10 prostate cancer (CRPC), a phenotype closely linked with metastasis and greatly reduced
11 survival [35]. Currently, there are six approved treatments that demonstrate a survival
12 advantage in patients with metastatic CRPC, each of these target diverse aspects of the
13 disease [76]. The taxane family members docetaxel and cabazitaxel interact with micro-
14 tubule stability [19, 90], while abiraterone [76] or enzalutamide [78] interfere with androgen
15 signaling by blocking androgen formation or nuclear translocation, respectively. Other ap-
16 proved treatments are non-specific to PCa. For example, general treatments such as
17 sipuleucel-T, a first generation cancer vaccine [45], and radium-223, an alpha emitter
18 which targets bone metastasis [68], are both approved to treat CRPC. Unfortunately, re-
19 gardless of the therapeutic approach, the survival advantage of these treatments is typi-
20 cally only a few months. Thus, understanding the molecular basis of the loss of androgen
21 sensitivity in CRPC could be an important step for the development of the next generation
22 of therapies with a prolonged survival advantage.

23 Androgen-induced proliferation and survival depends upon many coordinated signal
24 transduction and gene expression events. Androgen Receptor (AR) is part of the nu-
25 clear hormone receptor superfamily, which includes other important cancer targets such
26 as progesterone receptor (PR) and estrogen receptor (ER) in breast cancer [2]. Nuclear

27 hormone receptors act as ligand dependent transcription factors interacting with specific
28 DNA sequences of target genes as either monomers, heterodimers, or homodimers; AR,
29 PR, and ER act as homodimers. In the case of AR these specific DNA sequences are
30 known as androgen response elements (ARE) [61]. In the absence of androgen, AR
31 is predominately found in the cytoplasm bound to heat shock proteins (HSP) [74]. An-
32 drogen, either testosterone or testosterone metabolites such as 5α -dihydrotestosterone
33 (DHT), enter prostate cells and interact with the cytosolic androgen receptor (AR). The in-
34 teraction of DHT with AR promotes the dissociation of AR from chaperones such as HSP
35 [73] and its subsequent dimerization, phosphorylation and translocation to the nucleus
36 (reviewed by Brinkmann *et al.* [4]). Activated nuclear AR drives a gene expression pro-
37 gram broadly referred to as androgen action, that promotes both proliferation and survival.
38 In addition to many genes including itself, activated nuclear AR promotes the expression
39 and secretion of prostate specific antigen (PSA), arguably the best known PCa biomarker
40 [22]. PSA is commonly used as a prostate cancer indicator, although its prognostic ability
41 is controversial [3, 41, 65]. In CRPC, AR signals in the absence of androgens. Andro-
42 gen dependent (AD) prostate cells can become castration resistant (CR) through several
43 possible mechanisms, including constitutively amplified AR expression and altered AR
44 sensitivity to testosterone or other non-androgenic molecules [22]. In this study, we fo-
45 cused on the aberrant activation of AR by kinase signaling cascades, sometimes called
46 the outlaw pathway. Outlaw pathway activation is driven by over-activated receptor tyro-
47 sine kinases (RTKs), a common pathology in many cancer types including PCa [16, 83].
48 RTKs stimulate downstream kinases, including the AKT and mitogen-activated protein
49 kinase (MAPK) pathways, which promote AR phosphorylation and dimerization in the ab-
50 sence of an androgen signal [16, 104]. Interestingly, among the few genes activated AR
51 represses is cellular prostatic acid phosphatase (cPAcP), itself a key regulatory of RTK ac-
52 tivation [95]. Thus, in CRPC the androgen program is initiated without the corresponding

53 extracellular hormone cue, potentially from crosstalk between growth factor and hormone
54 receptor pathways.

55 In this study, we developed a mathematical model of growth factor and hormone signal
56 integration in androgen dependent, intermediate and resistant prostate cancer cells. We
57 used this model to better understand which components and processes were differentially
58 important in AD versus CR cells. The new model architecture was a significant advance
59 over our previous prostate signaling model [91]. We added the regulated expression of ten
60 additional proteins, including the cell cycle restriction point proteins cyclin D (and the dif-
61 ferentially spliced variants cyclin D1a and cyclin D1b), cyclin E, cyclin-dependent kinase
62 inhibitor 1A (p21Cip1), and cyclin-dependent kinase inhibitor 1B (p27Kip1). Also, we in-
63 cluded the Rb/E2F pathway, expanded our description of the activation of the mammalian
64 target of rapamycin (mTOR) protein and its role in translation initiation, and included the
65 regulation of AR action by cyclin D1a and E2F. However, this upgraded architecture, while
66 increasing the biological scope of the model, also expanded the number of unknown
67 model parameters. To estimate these parameters, we used multiobjective optimization
68 in combination with dynamic and steady-state data sets generated in AD, intermediate
69 and CR LNCaP cell lines. We identified a population of approximately $N = 5000$ models
70 (from well over a million candidate models) which described both AD and CR data sets
71 using a single model structure. Furthermore, we tested the model using an additional 29
72 LNCaP data sets not used for model training, along with four drug studies. We analyzed
73 the model population using sensitivity and robustness analysis to uncover differentially
74 important mechanisms in AD versus CR cell lines. In the presence of androgen, the sen-
75 sitivity profile was similar between AD and CR cells. Components of the MAPK and PI3K
76 pathways were highly fragile, irrespective of the level of androgen dependence. However,
77 in the absence of androgen, there were 609 statistically significant shifts in species sen-
78 sitivity between AD and CR cells. Of these, 108 were larger than one standard deviation

79 above the mean. In CR cells, HER2 activation of the MAPK and PI3K pathways was
80 significantly more important, as was AR activation through the MAPK pathway. On the
81 other hand, components of the translation and transcription infrastructure were differen-
82 tially more important in AD cells in the absence of androgen. Taken together, our analysis
83 suggested that independently targeting the PI3K or MAPK pathways in combination with
84 anti-androgen therapies could perhaps be an effective treatment strategy for CRPC.

85 **Results**

86 **Estimating an ensemble of prostate signaling models.** We modeled the integration
87 of growth factor, cell cycle and hormone signaling pathways in AD and CR LNCaP cells
88 (Fig. 1). The signaling architecture was hand curated from over 80 primary literature
89 sources in combination with biological databases. The model equations were formulated
90 as a system of ordinary differential equations (ODEs), where biochemical reaction rates
91 were modeled using mass action kinetics. ODEs and mass action kinetics are common
92 modeling tools [97], however, ODEs have the disadvantage of requiring estimates for
93 unknown model parameters. Many techniques have been developed to estimate ODE
94 model parameters, often from noisy and sparse experimental data [64]. Typically these
95 identification problems are underdetermined, hence no unique parameter values can be
96 estimated [96]. Thus, instead of estimating a single yet highly uncertain parameter set, we
97 estimated an ensemble of possible parameter sets using the Pareto Optimal Ensemble
98 Techniques (POETs) algorithm [85]. POETs uses a combination of simulated annealing
99 and local optimization techniques coupled with Pareto optimality-based ranking to simul-
100 taneously optimize multiple objective functions. Starting from an initial best fit set, we
101 estimated the 1687 unknown model parameters (1674 kinetic parameters and 13 non-
102 zero initial conditions) using 43 *in vitro* data sets taken from AD, intermediate and CR
103 LNCaP cells (Table T1). Each of the 43 training data sets was a separate objective in the
104 multiobjective calculation. The training data were steady-state or dynamic immunoblots
105 from which we extracted relative species abundance from their optical density profiles.
106 POETs sampled well over a million possible parameter sets, from which we selected N
107 = 5000 sets for further analysis. Over the ensemble, the coefficient of variation (CV) of
108 the kinetic parameters spanned 0.59 - 5.8, with 33% of the parameters having a CV of
109 less than one (Fig. S1). As a control, we also performed simulations for R = 100 random
110 parameter sets to compare against the ensemble generated by POETs.

The ensemble of PCa models recapitulated training data in both AD and CR cell lines with only two experimentally justified parameter changes (Fig. 2 and Fig. 3). Data from the LNCaP clones C-33 (dependent), C-51 (intermediate), and C-81 (resistant) [42, 44, 55] along with the CR LNCaP cell lines LNCaP-Rf [66], LNCaP-AI [11] and LNAI [27] were used for model identification. To simulate the effective difference between LNCaP cell lines, the parameter controlling the maximum rate of PAcP gene expression was scaled by 0.1 and 0.5, respectively, for the C-81 and C-51 cell-lines compared to C-33. This modification was based upon steady-state PAcP data from the three LNCaP clones [50]. Similarly, the expression of p16INK4 was adjusted in accordance with the study of Lu *et al.* [60]. These two parameters were the only adjustable parameter differences between AD and CR cells. To simulate an increased mTOR activation in the presence of a DHT stimulus, we added a first order activation term for mTOR activation with a DHT stimulus. Androgens have been shown to increase expression of proteins involved in cellular metabolism, which may lead to an increase in mTOR activation [102]. The model fit 36 of the 43 training objectives for greater than 40% of the ensemble members (Fig. 2A). Conversely, only 10 of the 43 training objectives were captured with the random parameter control (Fig. 2B). The model captured the crosstalk between RTK activation and androgen action (Fig. 3). The model described DHT-induced PSA expression in both C-33 (Fig. 3A) and C-81 (Fig. 3B) cells. Interestingly, simulations with the HER2 inhibitor AG879 recapitulated decreased PSA expression in C-81 cells (Fig. 3C) in the absence of androgen stimulation. AR action decreased the PAcP mRNA message (Fig. 3D), presumably leading to increased HER2 activity. The model also recapitulated the integration of androgen action with AR expression, G1/S cell cycle protein expression and AKT phosphorylation. For example, the model captured AR-induced AR expression following a DHT stimulus (Fig. 3H). Conversely, the transcription factor E2F inhibits AR transcription in LNCaP cells (Fig. 3I). Other cell cycle proteins were also integrated with

137 androgen action. For example, the cyclin D1 abundance increased in CR compared to
138 AD cells in the absence of androgen (Fig. 3E), while DHT induced p21Cip1 expression
139 in C-33 cells (Fig. 3F). The level of phosphorylated AKT was also increased in higher
140 passage number cells (Fig. 3G). Taken together, [FINISH ME].

141 **Validation simulations revealed missing network structure.** The model was vali-
142 dated against 29 *in vitro* and four *in vivo* studies (Table T2). For 15 of the 29 cases,
143 greater than 40% of the ensemble was qualitatively consistent with the experimental data
144 (Fig. 2C). However, for the random parameter control, only 7 of the 29 cases were sat-
145 isfied (Fig. 2D). We correctly predicted positive feedback between HER2 auto-activation
146 and androgen action (Fig. 4A and Fig. 4B). We also captured the dose-dependence of
147 AR abundance on DHT (Fig. 4C). In addition to the cell line studies, we simulated the
148 outcome of enzalutamide, lapatinib, and sorafenib clinical trials in AD and CRPC patients.
149 The trial end points were the reduction in PSA expression relative to an untreated base-
150 line. Enzalutamide acts on AR by inhibiting its nuclear translocation, DNA binding, and
151 coactivator recruitment [78]. In the enzalutamide trial, 54% of the patients that received
152 the drug showed a PSA decline of $\geq 50\%$ while 25% showed a decline $\geq 90\%$. We
153 simulated enzalutamide exposure by reducing the rate constants governing activated AR
154 binding to nuclear importer, cyclin E, and CDK6 to 1% of their initial values. Consistent
155 with the trial, 62% of ensemble members showed a $\geq 50\%$ decline in PSA abundance,
156 while 14% showed a $\geq 90\%$ decline (Fig. 4G). The second trial we simulated involved ex-
157 posure of CRPC patients to sorafenib. Sorafenib is a kinase inhibitor with activity against
158 Raf, vascular endothelial growth factor receptor (VEGFR), platelet-derived growth factor
159 receptor (PDGFR), c-kit and c-Ret [17]. We considered only the effects of sorafenib on the
160 protein kinase Raf, as VEGFR, PDGFR, c-kit and c-Ret were not included in the model.
161 None of the 22 patients in the sorafenib study showed a PSA decline of $> 50\%$. However,
162 our simulations showed that approximately 55% of the ensemble members had a PSA

163 decline of $\geq 50\%$. The last drug we considered was lapatinib, an inhibitor of epidermal
164 growth factor receptor (EGFR) and HER2 tyrosine kinase activity [58]. Two lapatinib drug
165 trials were considered: one in which patients had CRPC and one in which patients had
166 biochemically relapsed ADPC [58, 100]. In the CRPC lapatinib drug trial, two of the 21 en-
167 rolled patients had a PSA response $\geq 47\%$ [100]. For the CRPC case, our model showed
168 26.5% of ensemble members with a PSA response $\geq 47\%$. Of the 35 patients enrolled in
169 the ADPC lapatinib study, no PSA decreases was observed [58]. In this case, our model
170 showed 9.2% of ensemble members with a PSA response $\geq 50\%$. Although no response
171 to lapatinib was seen in ADPC clinical trials, *in vitro* AD LNCaP experiments showed de-
172 creased PSA expression in response to lapatinib, most notably with the addition of DHT
173 [59].

174 Validation and training failures suggested the original signaling architecture was miss-
175 ing critical components. Several of the failed training and validation simulations involved
176 the response of the network to epidermal growth factor (EGF) stimulation. For example,
177 Chen *et al.* showed that HER2 phosphorylation increased within five minutes following
178 EGF stimulation of LNCaP-AI cells [11]. We predicted no connection between HER2
179 phosphorylation and EGF stimulation on this short timescale (Fig. 4E). Interestingly, we
180 initially neglected the heterodimerization of HER2 with other ErbB family members in or-
181 der to simplify the model. However, Chen *et al.* suggested that HER2-EGFR heterodimer-
182 ization could be an important factor in EGF-driven activation of HER2 [11]. We tested this
183 hypothesis by developing a new model that included HER2 and EGFR heterodimeriza-
184 tion. We set the rate constants governing the assembly of HER2/EGFR heterodimers
185 equal to EGFR homodimer assembly; all other parameters were unchanged. This was
186 a reasonable first approximation, as the affinity of HER2/EGFR heterodimerization and
187 EGFR homodimerization is thought to be similar [39]. With the inclusion of HER2-EGFR
188 heterodimerization, we qualitatively fit the EGF-induced HER2 activation case and im-

189 proved our training for experiments that involved an EGF stimulus, e.g., cyclin D mRNA
190 and protein abundance following an EGF stimulus in C-33 cells (Fig. 2A and C, white
191 pixels and Fig. S2).

192 **Sensitivity analysis identified differentially important features of the prostate ar-**
193 **chitecture.** We used sensitivity analysis to identify important signaling components in
194 AD versus CR cells (Fig. 5). We calculated first order steady-state sensitivity coefficients
195 under different stimuli for 500 parameter sets selected from the ensemble. Signaling com-
196 ponents were rank-ordered based upon analysis of their sensitivity coefficient values. In
197 the presence of DHT, the sensitivity profile was similar for AD versus CR cells, with only a
198 few differences (Fig. 5B). The top 2% of sensitive species, regardless of androgen depen-
199 dence, involved components from the MAPK and PI3K pathways. In particular, activated
200 Ras, Raf, phosphorylated MEK, as well as PIP3 localized AKT, phosphorylated AKT, and
201 PI3K were sensitive in both AD and CR cells. Species involving PAcP and p16INK4 were
202 more sensitive in AD cells, which was expected since the expression of these two proteins
203 were the only parameters changed between AD and CR cells. Other species such as E2F,
204 cyclin E, and DHT-activated AR were also more sensitive in AD cells. On the other hand,
205 HER2-Grb2-Gab activation of PI3K and AKT inhibition of Raf were more sensitive in CR
206 cells.

207 The importance of signaling components varied with androgen dependence in the ab-
208 sence of DHT (Fig. 5A). There were 609 statistically significant shifts in species sensitivity
209 (318 more and 291 less sensitive) between CR and AD cells in a non-androgen environ-
210 ment. However, only 108 of these shifts were greater than one standard deviation above
211 the mean. In CR cells, HER2 activation of ERK and PI3K was more sensitive, as was AR
212 activation through the MAPK pathway. This was expected, as outlaw pathway activity was
213 elevated in castration resistant cells. Species in the MAPK pathway were in general more
214 sensitive in CR cells (128 out of 140 significant), with all forms of sPAcP more robust in

215 CR cells. On the other hand, infrastructure pathways encoding transcription and transla-
216 tion were more sensitive in AD cells. PSA and cyclin D1b (mRNA and mRNA complexes)
217 were the only species involved in translation that were more robust in AD cells (14 out of
218 116). The transcription factor, E2F was more fragile in AD cells, while the transcription
219 factors ETS and AP1 were more robust. ETS and AP1 are activated by phosphorylated
220 ERK, and ETS is also activated by active PKC [57, 101]. E2F is deactivated through bind-
221 ing to Rb, which is deactivated by cyclin D1 and CDK phosphorylation [48]. The model
222 also included AP1 suppression of AR transcriptional activity (more sensitive in CR) [77],
223 as well as inhibition of transcription of the AR gene by E2F (more sensitive in AD) [18].
224 Species in the PI3K pathway that were more fragile in AD cells included Rheb and TOR
225 complexes. Interestingly, these species were included as the last step in the PI3K path-
226 way prior to translation, with the phosphorylation of 4E-BP1 by TOR being considered the
227 beginning of translation in this model. This again indicates that in the absence of DHT
228 general translation is more fragile in AD cells.

229 There was a large shift in sensitive species between an androgen and a non-androgen
230 environment in both AD and CR cell lines (Fig. 5C and Fig. S3). Of the 664 statis-
231 tically significant shifts in AD cells, 288 were more sensitive between androgen versus
232 non-androgen environments. However, only 119 shifts were larger than one standard
233 deviation above the mean. Unsurprisingly, AR activation through DHT binding, with and
234 without coactivators, in a DHT environment was more sensitive, as was AR inhibition of
235 PAcP transcription (repressed by AR in the model). Species further upstream, such as
236 HER2 activation of the MAPK and PI3K/AKT pathways, were also more sensitive in a DHT
237 environment. Cell cycle species that were more fragile in the presence of DHT, included
238 complexes involving p21Cip1 and CDC25A. In a non-androgen environment, basal tran-
239 scription (68 out of 72) and translation (114 out of 120) were more fragile. Other fragile
240 species in the absence of DHT included Rb, E2F, Sam68, cyclin D1a complexes, phos-

241 phatases in the MAPK pathway, Rheb complexes, and TOR complexes.

242 We also considered the sensitivity of CR cells following the application of the AR in-
243 hibitor enzalutamide in the presence of DHT (Fig. 5D). Species which were more sen-
244 sitive in an androgen environment with enzalutamide included cytosolic AR, cPAcP, and
245 p21Cip1. As we would expect, AR species found in the nucleus and/or bound to coactiva-
246 tors, were more robust in the absence of enzalutamide. The top two percent of sensitive
247 species with and without enzalutamide were conserved. In a CR cell, enzalutamide had
248 no effect on the sensitivity of PI3K/AKT species as well as many MAPK species (ERK,
249 Raf, and MEK). Next, we looked at the effect of enzalutamide on a CR cell in both a non-
250 androgen and DHT environment (Fig. S3). More sensitive species in a non-androgen
251 environment included dimerized HER2, ERK, and PAcP. Species which were more ro-
252 bust in the non-androgen environment included, AR activated by DHT, AKT, p70, and
253 AR bound to HSP. The results of our sensitivity analysis indicate that instead of inhibiting
254 solely the AR pathway (enzalutamide), a combination therapy targeting the PI3K or MAPK
255 pathways in addition to AR may be more effective.

256 **Robustness analysis identified key regulators of prostate cancer.** Robustness anal-
257 ysis was conducted for 80 proteins to quantify the effects of amplifying or knocking down
258 key model components in both AD and CR cells. Gene expression parameters were al-
259 tered by a factor 10, 0.5, and 0 for knock-in, knock-down, or knock-out perturbations,
260 respectively. We calculated the effect of these perturbations on different protein markers,
261 such as PSA, AR, and cyclin D. A knock-out of Raf, MEK or ERK showed an overall in-
262 crease in cyclin D levels in CR cells (Fig. S4). This was unexpected and we saw a similar
263 increase in cyclin D due to the knock-in of Raf, MEK or ERK. We found that individual
264 ensemble members showed different response to a Raf knock-out, in both cyclin D con-
265 centration and PSA concentration. Of the 500 ensemble members, 126 members saw an
266 increase in PSA concentration and 62 members saw an increase in cyclin D concentra-

267 tion due to the knock-out of Raf (Fig. 6). We saw three distinct regions: (1) increase in
268 PSA concentration, (2) increase in cyclin D concentration, and (3) a decrease in both PSA
269 and cyclin D. We explored the flux vectors of the outlying parameter sets to understand
270 the mechanistic effect of Raf knock-out on PSA and cyclin D. Outlying parameter sets in
271 region 1 displayed high activation of PI3K through HER2 signaling as well as high asso-
272 ciation of AP1 with AR. AP1 binds and suppresses AR transcriptional activity in LNCaP
273 cells [77]. Knocking out Raf lowered AP1 levels and, therefore, freed AR for increased
274 transcription of PSA. In region 2, parameter sets also had high activation of PI3K through
275 HER2. They also had higher association of E2F with Rb and cyclin D1a with AR. Cyclin D
276 levels in this region increase due to an increase in E2F levels caused by the Raf knock-out.
277 Parameters in region 3 have high association of TOR. Interestingly, the drug sorafenib, a
278 multi-kinase inhibitor that has activity against Raf, showed no measurable PSA decline
279 in prostate cancer patients in clinical trials [17]. The robustness analysis showed that
280 network perturbation can result in unexpected responses due to cell-to-cell heterogeneity
281 in gene expression. These outlying cell types could be critical for understanding when
282 designing drug targets and combination therapies.

283 We also used robustness analysis to observe the effect of knocking out combinations
284 of key species found in our sensitivity analysis. We calculated the effect of perturbation
285 in CR cells on different protein markers in the following 7 cases: (1) Raf knock-out, (2)
286 PI3K knock-out, (3) AR knock-out, (4) Raf and PI3K knock-outs, (5) Raf and AR knock-
287 outs, (6) PI3K and AR knock-outs, and (7) Raf, PI3K and AR knock-outs. Over the 500
288 ensemble member set, the overall decrease in PSA expression levels was greatest in
289 all cases which included the knock-out of AR (Fig. 7A). The decreased expression of
290 activated p70 was most prominent in the double PI3K/AR knock-out case and the triple
291 Raf/PI3K/AR knock-out case (Fig. 7B). Although the change in expression level of cyclin
292 D varied for individual ensemble members (increased and decreased), the median and

mean behavior for all knock-out cases is around zero suggesting no change due to perturbation (Fig.7C). Individual ensemble members do show a decline in cyclin D expression in cases involving PI3K in double and triple knock-outs and in these cases we also see fewer ensemble members that have an increased expression of cyclin D. Fig. 7D shows that in the PI3K knock-out case we see a complete inhibition of AKTp expression (a value of -1 is essentially zero expression due to knock-out). This is a trivial result in the model because AKTp only occurs through PIP3 recruitment to the membrane, and PIP3 is only activated by PI3K in the model. All other knock-out cases show a median response of no fold change in AKTp expression, but we do see a group of ensemble members that have an increased expression of AKTp in the RAF knock-out and RAF/AR knock-out cases. Overall, these results are consistent with our hypothesis that a combination therapy will be more effective.

Experimental results confirm the need for dual therapies in prostate cancer. The results from our sensitivity analysis indicate that instead of inhibiting solely the AR pathway (enzalutamide), a combination therapy is necessary. To test this hypothesis we used the well characterized ADPC cell line LNCaP as well a LNCaP derived CRPC cell line C4-2 [93]. Three inhibitors were used: the AR inhibitor MDV3100 (enzalutamide), the Raf kinase inhibitor sorafenib, and the PI3K inhibitor LY294002. In both cell lines, inhibition of either the AR or MAPK pathway appears to promote activation of the PI3K pathway, as seen by the increase in pAKT (S473) (Fig. 8A). The addition of the PI3K inhibitor, LY294002, alone or in combination diminishes PI3K activity. The inhibition of PI3K alone, led to an increase in AR expression in both LNCaP and C4-2 cell lines. Since, AR transcriptionally upregulates its own expression [53][26], this may indicate an increase in AR activity. The ribosomal protein pS6 was completely inhibited only in the presence of the PI3K inhibitor LY294002. Cell viability results show a large decrease in cell viability at 72 hrs in the dual inhibition cases as well as the triple inhibition case for both LNCaP and

319 C4-2 cell lines (Fig. 8B). In both cell lines, MDV3100 (10 μ M), has only a modest effect
320 on cell viability versus control (DMSO). Figure 8C shows cell viability of both cell lines in
321 varying concentrations of inhibitors at 24 hrs.

322 **Discussion**

323 In this study, we developed a population of mathematical models describing growth fac-
324 tor and hormone signal integration in androgen dependent, intermediate and resistant
325 prostate cancer cells. These models described the regulation of androgen receptor ex-
326 pression and activation through androgen binding as well as a ligand-independent, MAPK-
327 driven mechanism referred to as the outlaw pathway. An ensemble of model parameters
328 was estimated using 43 steady-state and dynamic data sets taken from androgen depen-
329 dent, intermediate and independent LNCaP cell lines using multiobjective optimization.
330 Further, we tested the predictive power of the model by comparing model predictions
331 against 33 novel data sets (including four *in vivo* drug studies) not used during model
332 training. The model ensemble captured 84% of the training data and 52% of the validation
333 data relative to 23% and 24% for a random control population. Interestingly, during the the
334 initial round of parameter estimation, we identified several potentially missing structural
335 components not present in the original connectivity. One such component, EGF-induced
336 HER2/EGFR heterodimerization, was added to the current generation model. Inclusion of
337 this structural component significantly improved both training and validation performance
338 using the same rate constants as the EGFR-homodimer case (no additional parameter
339 fitting). We then analyzed the population of signaling models, using both sensitivity and
340 robustness analysis, to identify the critical components controlling network performance
341 in a variety of conditions.

342 In addition, three of the validation cases involved the effect of EGF on AR and AR-
343 activated genes, i.e., PSA. Cai *et al.* showed decreased expression of endogenous AR

344 as well as androgen-regulated PSA in AD LNCaP cells due to an EGF stimulus [8]. Cinar
345 *et al.* also showed decreased AR protein expression due to EGF, an effect reversed by
346 the mTOR inhibitor, Rapamycin [15]. Model simulations show either the opposite trend
347 or no effect due to EGF stimulus (Fig. 4F) [15]. These results suggest missing network
348 structure. From additional literature searches, the inhibition of AR activation through EGF
349 is still an open question, with many groups debating the biology involved, predominately
350 in the PI3K/AKT pathway. Lin *et al.* found that in low passage number LNCaP cells (C-
351 33), AKT negatively regulates AR by destabilizing it and marking it for ubiquitylation. In
352 high passage number LNCaP (C-81), AKT levels are high which contribute to AR stability
353 and less degradation [53]. Wen *et al.* showed that HER2 could induce AKT activation and
354 LNCaP cell growth in the presence and absence of androgen [99]. Another study shows
355 AKT phosphorylation of AR at S213 and S790 suppresses AR transactivation and AR-
356 mediated apoptosis of LNCaP [54]. The study from Cai *et al.* showed the reduction in AR
357 was not due to degradation or PI3K/AKT signaling, but instead was due to decreased AR
358 mRNA levels [8]. They found that AR protein levels in CR cells were not affected by EGF.
359 Others though have found that PSA expression, even in C-81 cells, is decreased by EGF
360 [33]. In other prostate cell lines, EGF has been shown to increase AR transactivation
361 [29, 72]. The MAPK pathway, which is downstream of EGFR, may also enhance AR
362 responses to low levels of androgen [31, 98]. Due to the discrepancies in the literature,
363 experiments should be performed before adding additional network connectivity to the
364 model.

365 The population of PCa models was analyzed using sensitivity analysis to identify key
366 signaling components and processes in both AD and CR cells. There was very little dif-
367 ference between sensitive and robust components in AD versus CR cells in the presence
368 of androgen. MAPK and PI3K pathway components were consistently ranked in the top
369 2% of sensitive species in the presence of androgen for both AD and CR cells. On the

other hand, cell cycle species, such as cyclin D-CDK4/6 complexes bound to cell cycle inhibitors (p27Kip1, p21Cip1, p16INK4), were consistently robust. However, this profile changed considerably in the absence of androgen. The activation of PI3K and ERK by HER2 dimerization and autophosphorylation was significantly more important in CR versus AD cells. Interestingly, AR activation by ERK was also more sensitive in CR versus AD cells in the absence of androgen. Lastly, although AR-regulated transcriptional processes were equally sensitive between the cell types, general translational and transcriptional components were more robust in CR versus AD cells. This evidence supports the current theory that CR cells will still respond to androgen and, thus, AR is still an active target in therapeutic against CRPC [46]. Supporting the argument that AR can be activated in the absence of androgens by MAPK activation [22]. Advanced prostate cancers often have higher levels of E2F and other transcription factors [18]. Interestingly, E2F was more sensitive in AD cells, while other transcription factors (ETS and AP1) were more robust. The drug enzalutamide had no effect on the top 2% of sensitive species. Species in the PI3K/AKT and MAPK pathways in the presence of enzalutamide were still highly sensitive. The application of enzalutamide, increased sensitivity of AR species found outside of the nucleus as well as PAcP species. Robustness analysis indicated diverse effects of Raf knock-out on PSA and cyclin D concentrations. Clinical studies of sorafenib, a multi-kinase inhibitor that has activity against Raf, showed increase PSA levels in patients [17]. Our results indicate that cell-to cell heterogeneity in gene expression can play a significant role in determining cell response. Thus, combination therapies need to be considered even in the case of a Raf knock-out.

The results of the model suggest that an inhibition of either the PI3K pathway or the MAPK pathway in combination with an AR inhibitor as a possible therapy for CRPC. Sensitivity analysis revealed no change in the top sensitive species in the presence or absence of the AR inhibitor, enzalutamide. PI3K/AKT and MAPK species continued to fall in the

396 top two percent of sensitive species. A study by Carver *et al.* looked at dual inhibition
397 of AR and PI3K signaling in LNCaP cells and in a Pten-deficient murine prostate cancer
398 model [68]. Using both the PI3K inhibitor, BEZ235, and the AR inhibitor, MDV3100 (en-
399 zalutamide), the group saw a drastic decrease in the total number of cells. Each inhibitor
400 on its own had a much smaller effect on total cell number. They saw an increase in the
401 cell death marker, c-PARP, in the dual inhibition case. The group hypothesized that AKT
402 inhibition leads to increased AR signaling activity through increased protein concentra-
403 tions of HER3. On the other hand AR inhibition leads to increased AKT activity due to the
404 down regulation of PHLPP, a protein phosphatase that regulates AKT. For the simplicity of
405 this model, the HER3 pathway and also cell death were not included in the model. Dual
406 knock-out studies of PI3K and AR in our model show only a slight additive effect on cell
407 cycle protein cyclin D through the dual knock-out compared to solely inhibiting PI3K (Fig.
408 7). The triple case, with PI3K, AR, and RAF knock-outs, also only showed a slight additive
409 effect (Fig. 7). This could indicate that the combined decrease in cell population due to
410 the dual inhibition of PI3K and AR is entirely due to cell death. The Carver *et al.* study
411 did not consider cell cycle proteins or cell growth. Our model does show a decrease in
412 cell cycle proteins in the PI3K knock-out as well as in the PI3K and AR dual knock-out
413 case in some ensemble members (Fig. 7). This result seems to be consistent with the
414 decreased cell count in the PI3K knock-out case which is not dependent on cell death,
415 as c-PARP levels are low. The decrease in cell cycle proteins in the model is due to a
416 decrease in general translation, including free eIF4E levels and activated 40S ribosome
417 subunit. The decrease in p70 (S6) activation due to inhibition of PI3K is shown in both the
418 model and in the Carver *et al.* study , indicating this result is due to the PI3K pathway (Fig.
419 S5). Our experimental results confirm the Carver *et al.* study in that a dual inhibition of
420 AR and PI3K signaling led to a more prominent decrease in cell viability then each of the
421 inhibitors alone in LNCaP cells. We extended the study to look at the addition of a third

422 inhibitor, sorafenib, that inhibits Raf kinase in the MAPK pathway and an additional cell
423 line, C4-2, which was CR. In both cell lines, there was not a significant decrease in cell
424 viability between the three dual inhibitor cases and the triple inhibition case at 74 hours,
425 indicating that a dual inhibition (PI3K/AR, AR/MAPK, or PI3K/MAPK) may be a sufficient
426 treatment.

427 The PCa signaling architecture was assembled after extensive literature review and
428 hand curation of the biochemical interactions. However, there are a number of areas
429 where model connectivity could be refined, e.g., the regulation of AR phosphorylation. We
430 assumed a single canonical activating AR phosphorylation site (S515), with ERK being
431 the major kinase and PP2A or PP1 being the major phosphatases responsible for regulat-
432 ing this site. MAPK activation following EGF treatment increases AR transcription and cell
433 growth, partially through AR phosphorylation on MAPK consensus site S515 [72]. How-
434 ever, there are at least 13 phosphorylation sites identified on AR, with phosphorylation at
435 six of these being androgen induced [25]. Moreover, other kinases such as AKT, protein
436 kinase C (PKC) family members, as well as Src-family kinases can all phosphorylate AR
437 in prostate cells [31, 72]. For example, AKT activation leads to AR phosphorylation at both
438 S213 and S791 (however, the role of these sites remains unclear) [53, 54, 89, 99]. AKT
439 effects on AR may also be passage number dependent, with AKT repressing AR transcrip-
440 tion in low passage number cells and enhancing transcription in higher passage numbers
441 [53]. Androgen independent phosphorylation of AR by Src family kinases (not currently in
442 model) at Y534 [31] or by protein kinase C (PKC) family members at the consensus site
443 S578 could also be important for understanding the regulation of AR activity. A second
444 area we will revisit is the gene expression program associated with androgen action, and
445 particularly the role of AR coregulators. Currently, we included only two AR coactivators,
446 cyclin E and CDK6 [52, 103] and three corepressors AP1, Cdc25A, and cyclin D1a in the
447 model [13, 71, 77]. However, there are at least 169 proteins classified as potential AR

448 coregulators [36, 37] with many of these being differentially expressed in malignant cells.
449 For example, the expression of steroid receptor coactivator-1 (Src-1) and transcriptional
450 intermediary factor 2 (Tif-2), both members of the steroid receptor coactivator family, are
451 elevated in prostate cancer [29, 30]. Src-1 is phosphorylated by MAPK and interacts di-
452 rectly with AR to enhance AR-mediated transcription [36]. Another class of potentially
453 important AR coregulators are the cell cycle proteins Cdc25 and Rb. Unlike Cdc25A,
454 Cdc25B (not in the model) can act as an AR coactivator leading to enhanced AR tran-
455 scription activity [67]. The Rb protein, in addition to being a key cell cycle regulator, has
456 been shown to be an AR coactivator in an androgen-independent manner in DU145 cells
457 [105]. However, there is some uncertainty about the role of Rb as Sharma *et al.* showed
458 that Rb decreased AR activation in multiple prostate cancer cell lines and xenografts [80].
459 Forkhead proteins have also been shown to activate as well as repress AR function. In
460 prostate cancer, AKT suppresses AFX/Forkhead proteins, which diminishes expression
461 of AFX target genes, such as p27Kip1 [6, 28, 62, 87]. Lastly, undoubtedly there are sev-
462 eral other signaling axes important in PCa, such as cytokine or insulin- and insulin-like
463 growth factor signaling [9, 38, 79, 88]. Understanding the pathways associated with these
464 signals and how they relate to the current model, may give us a more complete picture of
465 CR prostate cancer.

466 **Materials and Methods**

467 **Prostate model signaling architecture.** We modeled the expression, translation and
468 post-translational modifications of key components of the signaling architecture. The
469 model, which consisted of 780 protein, lipid or mRNA species interconnected by 1674
470 interactions, was a significant extension to our previous model [91] in several important
471 areas. First, we included well-mixed nuclear, cytosolic, membrane and extracellular com-
472 partments (including transfer terms between compartments). Next, we expanded the
473 description of growth factor receptor signaling, considering both homo- and heterodimer
474 formation between ErbB family members and the role of cellular and secreted prostatic
475 acid phosphatase (cPAcP and sPAcP, respectively). Both forms of PAcP were included
476 because cPAcP downregulates HER2 activity, while sPAcP promotes modest HER2 ac-
477 tivation [95]. Third, we expanded the description of the G1/S transition of the cell cycle
478 (restriction point). The previous model used the abundance of cyclin D as a proliferation
479 marker, but did not include other proteins or interactions potentially important to the re-
480 striction point. Toward this shortcoming, we included cyclin E expression (and its role as
481 a coregulator of androgen receptor expression), enhanced the description of cyclin D ex-
482 pression and the alternative splicing of cyclin D mRNA (including the role of the splice vari-
483 ants in androgen action), included the Rb/E2F pathway as well as E2F inhibition of andro-
484 gen receptor expression [18], and the cyclin-dependent kinases cyclin-dependent kinase
485 4 (CDK4) and cyclin-dependent kinase 6 (CDK6). We also included key inhibitors of the
486 restriction point including cyclin-dependent kinase inhibitor 1 (p21Cip1), cyclin-dependent
487 kinase inhibitor 1B (p27Kip1), and cyclin-dependent kinase inhibitor 2A (p16INK4) [81].
488 Fourth, we enhanced the description of growth factor induced translation initiation. One
489 of the key findings of the previous model was that growth factor induced translation ini-
490 tiation was globally sensitive (important in both androgen dependent and independent
491 conditions). However, the description of this important subsystem was simplified in the

492 previous model. Here, we expanded this subsystem, using connectivity similar to previ-
 493 ous study of Lequieu *et al.* [51], and re-examined the importance of key components of
 494 this axis, such as mammalian target of rapamycin (mTOR), phosphatidylinositide 3-kinase
 495 (PI3K) and AKT. Lastly, we significantly expanded the description of the role of androgen
 496 receptor. The previous model assumed constant AR expression, consistent with studies
 497 in androgen dependent and independent LNCaP sublines [50]. However, other prostate
 498 cancer cell lines vary in their AR expression [84]. Thus, to capture androgen signaling in
 499 a variety of prostate cancer cells, we included the transcriptional regulation governing an-
 500 drogen receptor expression, updated our description of the regulation of androgen recep-
 501 tor activity and androgen action (gene expression program driven by activated androgen
 502 receptor). At the expression level, we included AR auto-regulation in combination with the
 503 co-activators cyclin E and CDK6 [52, 103]. We also assumed androgen receptor could be
 504 activated through androgen binding or a ligand-independent, MAPK-driven mechanism
 505 referred to as the outlaw pathway [22, 104]. We assumed a single canonical activating
 506 AR phosphorylation site (S515), with phosphorylated extracellular-signal-regulated kinase
 507 1/2 (ppERK1/2) being the major kinase and protein phosphatase 2 (PP2A) or phospho-
 508 protein phosphatase 1 (PP1) being the major phosphatases responsible for regulating this
 509 site. Finally, we modeled androgen receptor induced gene expression, including prostate
 510 specific antigen (PSA), cPAcP and p21Cip1.

511 **Formulation and solution of the model equations.** The prostate model was formu-
 512 lated as a coupled set of non-linear ordinary differential equations (ODEs):

$$\frac{dx}{dt} = S \cdot r(x, k) \quad x(t_o) = x_o \quad (1)$$

513 The quantity x denotes the vector describing the abundance of protein, mRNA, and other
 514 species in the model (780×1). The stoichiometric matrix S encodes the signaling architec-

515 ture considered in the model (780×1674). Each row of \mathbf{S} describes a signaling component
 516 while each column describes a particular interaction. The (i, j) element of \mathbf{S} , denoted by
 517 σ_{ij} , describes how species i is involved with interaction j . If $\sigma_{ij} > 0$, species i is produced
 518 by interaction j . Conversely, if $\sigma_{ij} < 0$, then species i is consumed in interaction j . Lastly,
 519 if $\sigma_{ij} = 0$, then species i is not involved in interaction j . The term $\mathbf{r}(\mathbf{x}, \mathbf{k})$ denotes the vec-
 520 tor of interactions rates (1674×1). Gene expression and translation processes as well as
 521 all biochemical transformations were decomposed into simple elementary steps, where
 522 all reversible interactions were split into two irreversible steps (supplemental materials).
 523 We modeled each network interaction using elementary rate laws where all reversible in-
 524 teractions were split into two irreversible steps. Thus, the rate expression for interaction q
 525 was given by:

$$r_q(\mathbf{x}, k_q) = k_q \prod_{j \in \{\mathbf{R}_q\}} x_j^{-\sigma_{jq}} \quad (2)$$

526 The set $\{\mathbf{R}_q\}$ denotes reactants for reaction q , while σ_{jq} denotes the stoichiometric co-
 527 efficient (element of the matrix \mathbf{S}) governing species j in reaction q . The quantity k_q
 528 denotes the rate constant (unknown) governing reaction q . Model equations were gen-
 529 erated in the C-programming language using the UNIVERSAL code generator, starting
 530 from an text-based input file (available in supplemental materials). UNIVERSAL, an open
 531 source Objective-C/Java code generator, is freely available as a Google Code project
 532 (<http://code.google.com/p/universal-code-generator/>). Model equations were solved us-
 533 ing the CVODE solver in the SUNDIALS library [40] on an Apple workstation (Apple,
 534 Cupertino, CA; OS X v10.6.8).

535 We ran the model to steady-state before calculating the response to DHT or growth
 536 factor inputs. The steady-state was estimated numerically by repeatedly solving the model

537 equations and estimating the difference between subsequent time points:

$$\|\mathbf{x}(t + \Delta t) - \mathbf{x}(t)\|_2 \leq \gamma \quad (3)$$

538 The quantities $\mathbf{x}(t)$ and $\mathbf{x}(t + \Delta t)$ denote the simulated abundance vector at time t and
539 $t + \Delta t$, respectively. The L_2 vector-norm was used as the distance metric, where $\Delta t = 100$
540 hr of simulated time and $\gamma = 0.001$ for all simulations.

541 We estimated an ensemble of model parameter sets using the Pareto Optimal En-
542 semble Techniques (POETs) multiobjective optimization routine [51, 85, 86]. POETs min-
543 imized the residual between model simulations and 43 separate training objectives taken
544 from protein and mRNA signaling data generated in androgen dependent, intermediate
545 and independent LNCaP cell lines (Table T1). From these training objectives, POETs
546 generated $> 10^6$ candidate parameter vectors from which we selected $N = 5000$ Pareto
547 rank-zero vectors for further analysis. The set-to-set correlation between selected sets
548 was approximately 0.60, suggesting only modest similarity between ensemble members.
549 Approximately 33%, or 560 of the 1674 parameters had a coefficient of variation (CV) of
550 less than 1.0, where the CV ranged from 0.59 to 5.8 over the ensemble. Details of the
551 parameter estimation problem and POETs are given in the supplemental materials.

552 **Sensitivity and robustness analysis.** Steady-state sensitivity coefficients were calcu-
553 lated for $N = 500$ parameter sets selected from the ensemble by solving the augmented
554 kinetic-sensitivity equations [20]:

$$\begin{bmatrix} \mathbf{S} \cdot \mathbf{r}(\mathbf{x}, \mathbf{k}) \\ \mathbf{A}(t_s) \mathbf{s}_j + \mathbf{b}_j(t_s) \end{bmatrix} = \begin{pmatrix} \mathbf{0} \\ \mathbf{0} \end{pmatrix} \quad j = 1, 2, \dots, \mathcal{P} \quad (4)$$

555 where

$$s_{ij}(t_s) = \frac{\partial x_i}{\partial k_j} \Big|_{t_s} \quad (5)$$

556 for each parameter set. Steady-state was calculated as described previously. The quan-
 557 tity j denotes the parameter index, \mathbf{A} denotes the Jacobian matrix, and \mathcal{P} denotes the
 558 number of parameters in the model. The vector \mathbf{b}_j denotes the j th column of the matrix
 559 of first-derivatives of the mass balances with respect to the parameters. Steady-state
 560 sensitivity coefficients were used because of the computational burden associated with
 561 sampling several hundred parameters sets for each of the 1674 parameters. The steady-
 562 state sensitivity coefficients $\mathcal{N}_{ij} \equiv s_{ij}$ were organized into an array for each parameter set
 563 in the ensemble:

$$\mathcal{N}^{(\epsilon)} = \begin{pmatrix} \mathcal{N}_{11}^{(\epsilon)} & \mathcal{N}_{12}^{(\epsilon)} & \dots & \mathcal{N}_{1j}^{(\epsilon)} & \dots & \mathcal{N}_{1P}^{(\epsilon)} \\ \mathcal{N}_{21}^{(\epsilon)} & \mathcal{N}_{22}^{(\epsilon)} & \dots & \mathcal{N}_{2j}^{(\epsilon)} & \dots & \mathcal{N}_{2P}^{(\epsilon)} \\ \vdots & \vdots & & \vdots & & \vdots \\ \mathcal{N}_{M1}^{(\epsilon)} & \mathcal{N}_{M2}^{(\epsilon)} & \dots & \mathcal{N}_{Mj}^{(\epsilon)} & \dots & \mathcal{N}_{MP}^{(\epsilon)} \end{pmatrix} \quad \epsilon = 1, 2, \dots, N_\epsilon \quad (6)$$

564 where ϵ denotes the index of the ensemble member, P denotes the number of parameters,
 565 N_ϵ denotes the number of parameter sets sampled ($N = 500$) and M denotes the number
 566 of model species. To estimate the relative fragility or robustness of species and reactions
 567 in the network, we decomposed $\mathcal{N}^{(\epsilon)}$ using Singular Value Decomposition (SVD):

$$\mathcal{N}^{(\epsilon)} = \mathbf{U}^{(\epsilon)} \Sigma^{(\epsilon)} \mathbf{V}^{T,(\epsilon)} \quad (7)$$

568 Coefficients of the left singular vectors corresponding to largest $\theta \leq 15$ singular values of
 569 $\mathcal{N}^{(\epsilon)}$ were rank-ordered to estimate important species combinations, while coefficients of
 570 the right singular vectors were used to rank important reaction combinations. Only coeffi-
 571 cients with magnitude greater than a threshold ($\delta = 0.001$) were considered. The fraction

572 of the θ vectors in which a reaction or species index occurred was used to quantify its
 573 importance (sensitivity ranking). We compared the sensitivity ranking between different
 574 conditions to understand how control in the network shifted in different cellular environ-
 575 ments.

576 Robustness coefficients were calculated as shown previously [92]. Robustness coef-
 577 ficients denoted by $\alpha(i, j, t_o, t_f)$ are defined as:

$$\alpha(i, j, t_o, t_f) = \left(\int_{t_o}^{t_f} x_i(t) dt \right)^{-1} \left(\int_{t_o}^{t_f} x_i^{(j)}(t) dt \right) \quad (8)$$

578 Robustness coefficients quantify the response of a marker to a structural or operational
 579 perturbation to the network architecture. Here t_o and t_f denote the initial and final sim-
 580 ulation time respectively, while i and j denote the indices for the marker and the pertur-
 581 bation respectively. A value of $\alpha(i, j, t_o, t_f) > 1$, indicates increased marker abundance,
 582 while $\alpha(i, j, t_o, t_f) < 1$ indicates decreased marker abundance following perturbation j .
 583 If $\alpha(i, j, t_o, t_f) \sim 1$ the j th perturbation does not influence the abundance of marker i .
 584 Robustness coefficients were calculated (starting from steady-state) from $t_o = 0$ hr to
 585 $t_f = 72$ hr following the addition of 10nM DHT at t_o . For scaled log fold change we used
 586 the following equation:

$$\alpha_{scaled}(i, j) = \begin{cases} \frac{\log_{10}(\alpha(i, j))}{\max \log_{10}(\alpha(i))}, & \text{if } \log_{10}(\alpha(i, j)) \geq 0 \\ -\frac{\log_{10}(\alpha(i, j))}{\min \log_{10}(\alpha(i))}, & \text{if } \log_{10}(\alpha(i, j)) < 0 \end{cases} \quad (9)$$

587 A value of $\alpha_{scaled}(i, j) > 0$, indicates increased marker abundance, while $\alpha_{scaled}(i, j) < 0$
 588 indicates decreased marker abundance following perturbation j . If $\alpha_{scaled}(i, j) \sim 0$ the j th
 589 perturbation does not influence the abundance of marker i . A value of $\alpha_{scaled}(i, j) = 1$,
 590 indicates max increase of marker abundance, while $\alpha_{scaled}(i, j) = -1$ indicates the max
 591 decrease of marker abundance. Robustness coefficients were calculated for the same N

592 = 500 models selected for sensitivity analysis.

593 **Experimental Validation.**

594 **Cell culture and treatments** Androgen dependent LNCaP prostate cancer cells were
595 a gift from Dr. Brian Kirby (Cornell University), and the castration resistant C4-2 prostate
596 cancer cell line was purchased from MD Anderson Cancer Center, University of Texas.
597 Cell lines were maintained in RPMI 1640 media (Life Technologies, Inc., Grand Island,
598 NY) with 10% fetal calf serum (FBS; Hyclone) and 1x antibiotic/antimycotic (Sigma, St.
599 Louis, MO) in a 5% CO₂ humidified atmosphere at 37°C. The AR inhibitor MDV3100
600 (enzalutamide) and the Raf inhibitor sorafenib were purchased from SantaCruz Biotech-
601 nology (Santa Cruz, CA). The PI3K inhibitor LY294002 was purchased from Cell Signaling
602 Technologies (Danvers, MA, USA). All stock solutions were diluted in DMSO and stored
603 at -20°C (Sigma, St. Louis, MO). Stock solution concentrations for western blotting ex-
604 periments were 10 mM Sorafenib, 50 mM LY294002, and 10 mM MDV3100. For the cell
605 viability assays, stock solution concentrations were 0.5 mM Sorafenib, 4 mM LY294002,
606 and 1 mM MDV3100.

607 **Protein Extraction and Western Blot** LNCaP and C4-2 cells were seeded in 60 mm
608 dishes at a density of 4 x 10⁵. After 96 and 72 hrs, for LNCaP and C4-2 cells respec-
609 tively, the media was replaced with fresh media and drug treatments were added. After
610 24 hours, cells were washed twice in PBS buffer, scraped in 250 µL ice-cold lysis buffer
611 (Pierce, Rockford, IL) supplemented with protease and phosphatase inhibitors (Sigma, St.
612 Louis, MO), and lysed for 30 min on ice. Lysates were centrifuged at 13,000 rpm for 30
613 min at 4°C. After quantification of total protein by BCA assay, equal amounts of total pro-
614 tein lysates (25 µg) were resolved by SDS-PAGE and transferred onto PVDF membranes.
615 Membranes were blocked in 5% fat free milk and then probed with antibodies. The pri-
616 mary antibodies used for western blot analysis were pAKT Ser473, AKT, pS6 Ser240/244

617 , pERK Thr202/Tyr204, ERK, AR, cleaved PARP, and GAPDH were from Cell Signal-
618 ing Technologies (Danvers, MA, USA). For detection, enhanced chemiluminescence ECL
619 reagent (GE Healthcare, Pittsburgh, PA) was used and signals were visualized using the
620 ChemiDoc XRS system (Bio-Rad).

621 **MTT Assay** LNCaP and C4-2 cells were seeded at a density of 1×10^4 cells per well in 96
622 well plates. After 48 hrs the media was refreshed and drug treatments added. Cell growth
623 at 24, 48, and 72 hrs was determined using a 3-(4,5-dimethyl thiazol-2-yl)-2,5-diphenyl
624 tetrazolium bromide (MTT) assay. At the specified time point 10 μ L MTT reagent (stock of
625 5 mg/mL in PBS) was added to each well and the cells were further incubated for 4 hrs.
626 At 4 hrs, the media was removed and 50 μ L of dissolving reagent DMSO was added to
627 each well. After an additional 10 min incubation, the absorbance was measured at 540
628 nm on a microplate reader. Each reading was adjusted by subtracting the absorbance
629 value for the blank (media only) and the results were then scaled to the DMSO-treated
630 (control) case.

631 Acknowledgements

632 This study was supported by award number U54CA143876 from the National Cancer In-
633 stitute. The content is solely the responsibility of the authors and does not necessarily
634 represent the official views of the National Cancer Institute or the National Institutes of
635 Health. The authors acknowledge the financial support of the National Science Founda-
636 tion, award no. DGE-1045513, for a GK12 training grant entitled "Grass Roots: Advanc-
637 ing Education in Renewable Energy and Cleaner Fuels through collaborative graduate
638 fellow/teacher/grade-school student interactions." We would like to thank Timothy Chu,
639 Kyriakos Tsahalis, Spencer Davis, Rohit Yallamraju, Gongcheng Lu, and Yalin Zhao.

640 **References**

- 641 1. Abramoff M Magelhaes P RS (2004) Image processing with imagej. *Biophotonics Int* **11**: 36–42
- 642 2. Aranda A, Pascual A (2001) Nuclear and Hormone Receptors and Gene Expression. *Physiological Reviews* **81**: 1269–1304
- 643 3. Attard G, de Bono JS (2009) Prostate cancer: PSA as an intermediate end point in clinical trials. *Nat Rev Urol* **6**: 473–5
- 644 4. Brinkmann AO, Blok LJ, de Ruiter PE, Doesburg P, Steketee K, Berrevoets CA, Trapman J (1999) Mechanisms of androgen receptor activation and function. *J Steroid Biochem Mol Biol* **69**: 307–13
- 645 5. Brown KS, Sethna JP (2003) Statistical mechanical approaches to models with many poorly known parameters. *Phys Rev E Stat Nonlin Soft Matter Phys* **68**: 021904
- 646 6. Brunet A, Bonni A, Zigmond MJ, Lin MZ, Juo P, Hu LS, Anderson MJ, Arden KC, Blenis J, Greenberg ME (1999) Akt promotes cell survival by phosphorylating and inhibiting a Forkhead transcription factor. *Cell* **96**: 857–68
- 647 7. Busà R, Paronetto MP, Farini D, Pierantozzi E, Botti F, Angelini DF, Attisani F, Vespasiani G, Sette C (2007) The RNA-binding protein Sam68 contributes to proliferation and survival of human prostate cancer cells. *Oncogene* **26**: 4372–82
- 648 8. Cai C, Portnoy DC, Wang H, Jiang X, Chen S, Balk SP (2009) Androgen receptor expression in prostate cancer cells is suppressed by activation of epidermal growth factor receptor and ErbB2. *Cancer Res* **69**: 5202–9
- 649 9. Cardillo MR, Monti S, Di Silverio F, Gentile V, Sciarra F, Toscano V (2003) Insulin-like growth factor (IGF)-I, IGF-II and IGF type I receptor (IGFR-I) expression in prostatic cancer. *Anticancer Res* **23**: 3825–35
- 650 10. Carver BS, Chapinski C, Wongvipat J, Hieronymus H, Chen Y, Chandarlapaty S,

- 666 Arora VK, Le C, Koutcher J, Scher H, Scardino PT, Rosen N, Sawyers CL (2011)
667 Reciprocal feedback regulation of PI3K and androgen receptor signaling in PTEN-
668 deficient prostate cancer. *Cancer Cell* **19**: 575–86
- 669 11. Chen L, Mooso BA, Jathal MK, Madhav A, Johnson SD, van Spyk E, Mikhailova M,
670 Zierenberg-Ripoll A, Xue L, Vinall RL, deVere White RW, Ghosh PM (2011) Dual
671 EGFR/HER2 inhibition sensitizes prostate cancer cells to androgen withdrawal by
672 suppressing ErbB3. *Clin Cancer Res* **17**: 6218–28
- 673 12. Chen S, Kesler CT, Paschal BM, Balk SP (2009) Androgen receptor phosphorylation
674 and activity are regulated by an association with protein phosphatase 1. *J Biol Chem*
675 **284**: 25576–84
- 676 13. Chiu YT, Han HY, Leung SCL, Yuen HF, Chau CW, Guo Z, Qiu Y, Chan KW, Wang X,
677 Wong YC, Ling MT (2009) CDC25A functions as a novel Ar corepressor in prostate
678 cancer cells. *J Mol Biol* **385**: 446–56
- 679 14. Chuang TD, Chen SJ, Lin FF, Veeramani S, Kumar S, Batra SK, Tu Y, Lin MF (2010)
680 Human prostatic acid phosphatase, an authentic tyrosine phosphatase, dephospho-
681 rylates ErbB-2 and regulates prostate cancer cell growth. *J Biol Chem* **285**: 23598–
682 606
- 683 15. Cinar B, De Benedetti A, Freeman MR (2005) Post-transcriptional regulation of the
684 androgen receptor by Mammalian target of rapamycin. *Cancer Res* **65**: 2547–53
- 685 16. Craft N, Shostak Y, Carey M, Sawyers CL (1999) A mechanism for hormone-
686 independent prostate cancer through modulation of androgen receptor signaling by
687 the HER-2/neu tyrosine kinase. *Nat Med* **5**: 280–5
- 688 17. Dahut WL, Scripture C, Posadas E, Jain L, Gulley JL, Arlen PM, Wright JJ, Yu Y, Cao
689 L, Steinberg SM, Aragon-Ching JB, Venitz J, Jones E, Chen CC, Figg WD (2008)
690 A phase II clinical trial of sorafenib in androgen-independent prostate cancer. *Clin
691 Cancer Res* **14**: 209–14

- 692 18. Davis JN, Wojno KJ, Daignault S, Hofer MD, Kuefer R, Rubin MA, Day ML (2006)
693 Elevated E2F1 inhibits transcription of the androgen receptor in metastatic hormone-
694 resistant prostate cancer. *Cancer Res* **66**: 11897–906
- 695 19. de Bono JS, Oudard S, Ozguroglu M, Hansen S, Machiels JP, Kocak I, Gravis G, Bo-
696 drogi I, Mackenzie MJ, Shen L, Roessner M, Gupta S, Sartor AO, TROPIC Investi-
697 gators (2010) Prednisone plus cabazitaxel or mitoxantrone for metastatic castration-
698 resistant prostate cancer progressing after docetaxel treatment: a randomised open-
699 label trial. *Lancet* **376**: 1147–54
- 700 20. Dickinson R, Gelinas R (1976) Sensitivity analysis of ordinary differential equation
701 systems—A direct method. *Journal of Computational Physics* **21**: 123–143
- 702 21. Fang Z, Zhang T, Dizeyi N, Chen S, Wang H, Swanson KD, Cai C, Balk SP, Yuan
703 X (2012) Androgen Receptor Enhances p27 Degradation in Prostate Cancer Cells
704 through Rapid and Selective TORC2 Activation. *J Biol Chem* **287**: 2090–8
- 705 22. Feldman BJ, Feldman D (2001) The development of androgen-independent prostate
706 cancer. *Nat Rev Cancer* **1**: 34–45
- 707 23. Fonseca C FP (1993) Genetic algorithms for multiobjective optimization: Formu-
708 lation, discussion and generalization. In *Proceedings of the fifth international confer-
709 ence on genetic algorithms Citeseer* **423**: 416–423
- 710 24. Gadkar KG, Doyle 3rd FJ, Crowley TJ, Varner JD (2003) Cybernetic model predictive
711 control of a continuous bioreactor with cell recycle. *Biotechnol Prog* **19**: 1487–97
- 712 25. Gioeli D, Paschal BM (2012) Post-translational modification of the androgen recep-
713 tor. *Mol Cell Endocrinol* **352**: 70–8
- 714 26. Grad JM, Dai JL, Wu S, Burnstein KL (1999) Multiple androgen response elements
715 and a Myc consensus site in the androgen receptor (AR) coding region are involved
716 in androgen-mediated up-regulation of AR messenger RNA. *Mol Endocrinol* **13**:
717 1896–911

- 718 27. Graff JR, Konicek BW, Lynch RL, Dumstorf CA, Dowless MS, McNulty AM, Parsons
719 SH, Brail LH, Colligan BM, Koop JW, Hurst BM, Deddens JA, Neubauer BL, Stan-
720 cato LF, Carter HW, Douglass LE, Carter JH (2009) eIF4E activation is commonly
721 elevated in advanced human prostate cancers and significantly related to reduced
722 patient survival. *Cancer Res* **69**: 3866–73
- 723 28. Graff JR, Konicek BW, McNulty AM, Wang Z, Houck K, Allen S, Paul JD, Hbaiu A,
724 Goode RG, Sandusky GE, Vessella RL, Neubauer BL (2000) Increased AKT activ-
725 ity contributes to prostate cancer progression by dramatically accelerating prostate
726 tumor growth and diminishing p27Kip1 expression. *J Biol Chem* **275**: 24500–5
- 727 29. Gregory CW, Fei X, Ponguta LA, He B, Bill HM, French FS, Wilson EM (2004) Epi-
728 dermal growth factor increases coactivation of the androgen receptor in recurrent
729 prostate cancer. *J Biol Chem* **279**: 7119–30
- 730 30. Gregory CW, He B, Johnson RT, Ford OH, Mohler JL, French FS, Wilson EM (2001)
731 A mechanism for androgen receptor-mediated prostate cancer recurrence after an-
732 drogen deprivation therapy. *Cancer Res* **61**: 4315–9
- 733 31. Guo Z, Dai B, Jiang T, Xu K, Xie Y, Kim O, Nesheiwat I, Kong X, Melamed J, Han-
734 dratta VD, Njar VCO, Brodie AMH, Yu LR, Veenstra TD, Chen H, Qiu Y (2006) Reg-
735 ulation of androgen receptor activity by tyrosine phosphorylation. *Cancer Cell* **10**:
736 309–19
- 737 32. Ha S, Ruoff R, Kahoud N, Franke TF, Logan SK (2011) Androgen receptor levels
738 are upregulated by Akt in prostate cancer. *Endocr Relat Cancer* **18**: 245–55
- 739 33. Hakariya T, Shida Y, Sakai H, Kanetake H, Igawa T (2006) EGFR signaling path-
740 way negatively regulates PSA expression and secretion via the PI3K-Akt pathway in
741 LNCaP prostate cancer cells. *Biochem Biophys Res Commun* **342**: 92–100
- 742 34. Handl J, Kell DB, Knowles J (2007) Multiobjective optimization in bioinformatics and
743 computational biology. *IEEEACM Trans Comput Biol Bioinform* **4**: 279–92

- 744 35. Harris WP, Mostaghel EA, Nelson PS, Montgomery B (2009) Androgen deprivation
745 therapy: progress in understanding mechanisms of resistance and optimizing an-
746 drogen depletion. *Nat Clin Pract Urol* **6**: 76–85
- 747 36. Heemers HV, Tindall DJ (2007) Androgen receptor (AR) coregulators: a diversity of
748 functions converging on and regulating the AR transcriptional complex. *Endocr Rev*
749 **28**: 778–808
- 750 37. Heinlein CA, Chang C (2002) Androgen receptor (AR) coregulators: an overview.
751 *Endocr Rev* **23**: 175–200
- 752 38. Heinlein CA, Chang C (2004) Androgen receptor in prostate cancer. *Endocr Rev* **25**:
753 276–308
- 754 39. Hendriks BS, Opresko LK, Wiley HS, Lauffenburger D (2003) Quantitative analysis
755 of HER2-mediated effects on HER2 and epidermal growth factor receptor endocyto-
756 sis: distribution of homo- and heterodimers depends on relative HER2 levels. *J Biol
757 Chem* **278**: 23343–51
- 758 40. Hindmarsh A, Brown P, Grant K, Lee S, Serban R, Shumaker D, Woodward C
759 (2005) SUNDIALS: Suite of nonlinear and differential/algebraic equation solvers.
760 *ACM Transactions on Mathematical Software* **31**: 363–396
- 761 41. Hoffman RM (2011) Clinical practice. Screening for prostate cancer. *N Engl J Med*
762 **365**: 2013–9
- 763 42. Horoszewicz JS, Leong SS, Kawinski E, Karr JP, Rosenthal H, Chu TM, Mirand EA,
764 Murphy GP (1983) LNCaP model of human prostatic carcinoma. *Cancer Res* **43**:
765 1809–18
- 766 43. Huggins C (1967) Endocrine-induced regression of cancers. *Cancer Res* **27**: 1925–
767 30
- 768 44. Igawa T, Lin FF, Lee MS, Karan D, Batra SK, Lin MF (2002) Establishment and char-
769 acterization of androgen-independent human prostate cancer LNCaP cell model.

- 770 *Prostate* **50**: 222–35
- 771 45. Kantoff PW, Higano CS, Shore ND, Berger ER, Small EJ, Penson DF, Red-
772 fern CH, Ferrari AC, Dreicer R, Sims RB, Xu Y, Frohlich MW, Schellhammer PF,
773 IMPACT Study Investigators (2010) Sipuleucel-T immunotherapy for castration-
774 resistant prostate cancer. *N Engl J Med* **363**: 411–22
- 775 46. Karantanos T, Corn PG, Thompson TC (2013) Prostate cancer progression after
776 androgen deprivation therapy: mechanisms of castrate resistance and novel thera-
777 peutic approaches. *Oncogene*
- 778 47. Knudsen KE, Arden KC, Cavenee WK (1998) Multiple G1 regulatory elements con-
779 trol the androgen-dependent proliferation of prostatic carcinoma cells. *J Biol Chem*
780 **273**: 20213–22
- 781 48. Lapenna S, Giordano A (2009) Cell cycle kinases as therapeutic targets for cancer.
782 *Nat Rev Drug Discov* **8**: 547–66
- 783 49. Lee MS, Igawa T, Lin MF (2004) Tyrosine-317 of p52(Shc) mediates androgen-
784 stimulated proliferation signals in human prostate cancer cells. *Oncogene* **23**: 3048–
785 58
- 786 50. Lee MS, Igawa T, Yuan TC, Zhang XQ, Lin FF, Lin MF (2003) ErbB-2 signaling
787 is involved in regulating PSA secretion in androgen-independent human prostate
788 cancer LNCaP C-81 cells. *Oncogene* **22**: 781–96
- 789 51. Lequieu J, Chakrabarti A, Nayak S, Varner JD (2011) Computational modeling and
790 analysis of insulin induced eukaryotic translation initiation. *PLoS Comput Biol* **7**:
791 e1002263
- 792 52. Lim JTE, Mansukhani M, Weinstein IB (2005) Cyclin-dependent kinase 6 associates
793 with the androgen receptor and enhances its transcriptional activity in prostate can-
794 cer cells. *Proc Natl Acad Sci U S A* **102**: 5156–61
- 795 53. Lin HK, Hu YC, Yang L, Altuwaijri S, Chen YT, Kang HY, Chang C (2003) Suppres-

- 796 sion versus induction of androgen receptor functions by the phosphatidylinositol 3-
797 kinase/Akt pathway in prostate cancer LNCaP cells with different passage numbers.
798 *J Biol Chem* **278**: 50902–7
- 799 54. Lin HK, Yeh S, Kang HY, Chang C (2001) Akt suppresses androgen-induced apop-
800 tosis by phosphorylating and inhibiting androgen receptor. *Proc Natl Acad Sci U S
A* **98**: 7200–5
- 801 55. Lin MF, Lee MS, Garcia-Arenas R, Lin FF (2000) Differential responsiveness of pro-
802 static acid phosphatase and prostate-specific antigen mRNA to androgen in prostate
803 cancer cells. *Cell Biol Int* **24**: 681–9
- 804 56. Lin MF, Lee MS, Zhou XW, Andressen JC, Meng TC, Johansson SL, West WW,
805 Taylor RJ, Anderson JR, Lin FF (2001) Decreased expression of cellular prostatic
806 acid phosphatase increases tumorigenicity of human prostate cancer cells. *J Urol*
807 **166**: 1943–50
- 808 57. Lindemann RK, Braig M, Ballschmieter P, Guise TA, Nordheim A, Dittmer J (2003)
809 Protein kinase Calpha regulates Ets1 transcriptional activity in invasive breast can-
810 cer cells. *Int J Oncol* **22**: 799–805
- 811 58. Liu G, Chen YH, Kolesar J, Huang W, Dipaola R, Pins M, Carducci M, Stein M,
812 Bubley GJ, Wilding G (2013) Eastern Cooperative Oncology Group Phase II Trial of
813 lapatinib in men with biochemically relapsed, androgen dependent prostate cancer.
814 *Urol Oncol* **31**: 211–8
- 815 59. Liu Y, Majumder S, McCall W, Sartor CI, Mohler JL, Gregory CW, Earp HS, Whang
816 YE (2005) Inhibition of HER-2/neu kinase impairs androgen receptor recruitment to
817 the androgen responsive enhancer. *Cancer Res* **65**: 3404–9
- 818 60. Lu S, Tsai SY, Tsai MJ (1997) Regulation of androgen-dependent prostatic cancer
819 cell growth: androgen regulation of CDK2, CDK4, and CKI p16 genes. *Cancer Res*
820 **57**: 4511–6

- 822 61. Mangelsdorf DJ, Thummel C, Beato M, Herrlich P, Schütz G, Umesono K, Blum-
823 berg B, Kastner P, Mark M, Chambon P, Evans RM (1995) The nuclear receptor
824 superfamily: the second decade. *Cell* **83**: 835–9
- 825 62. Medema RH, Kops GJ, Bos JL, Burgering BM (2000) AFX-like Forkhead transcrip-
826 tion factors mediate cell-cycle regulation by Ras and PKB through p27kip1. *Nature*
827 **404**: 782–7
- 828 63. Meng TC, Lee MS, Lin MF (2000) Interaction between protein tyrosine phosphatase
829 and protein tyrosine kinase is involved in androgen-promoted growth of human
830 prostate cancer cells. *Oncogene* **19**: 2664–77
- 831 64. Moles CG, Mendes P, Banga JR (2003) Parameter estimation in biochemical path-
832 ways: a comparison of global optimization methods. *Genome Res* **13**: 2467–74
- 833 65. Moyer VA, U.S. Preventive Services Task Force (2012) Screening for prostate can-
834 cer: U.S. Preventive Services Task Force recommendation statement. *Ann Intern
835 Med* **157**: 120–34
- 836 66. Murillo H, Huang H, Schmidt LJ, Smith DI, Tindall DJ (2001) Role of PI3K signaling in
837 survival and progression of LNCaP prostate cancer cells to the androgen refractory
838 state. *Endocrinology* **142**: 4795–805
- 839 67. Ngan ESW, Hashimoto Y, Ma ZQ, Tsai MJ, Tsai SY (2003) Overexpression of
840 Cdc25B, an androgen receptor coactivator, in prostate cancer. *Oncogene* **22**: 734–9
- 841 68. Parker C, Nilsson S, Heinrich D, Helle SI, O'Sullivan JM, Fosså SD, Chodacki A,
842 Wiechno P, Logue J, Seke M, Widmark A, Johannessen DC, Hoskin P, Bottomley
843 D, James ND, Solberg A, Syndikus I, Kliment J, Wedel S, Boehmer S, *et al* (2013)
844 Alpha emitter radium-223 and survival in metastatic prostate cancer. *N Engl J Med*
845 **369**: 213–23
- 846 69. Paronetto MP, Cappellari M, Busà R, Pedrotti S, Vitali R, Comstock C, Hyslop T,
847 Knudsen KE, Sette C (2010) Alternative splicing of the cyclin D1 proto-oncogene is

- regulated by the RNA-binding protein Sam68. *Cancer Res* **70**: 229–39
70. Perry JE, Grossmann ME, Tindall DJ (1998) Epidermal growth factor induces cyclin D1 in a human prostate cancer cell line. *Prostate* **35**: 117–24
71. Petre-Draviam CE, Cook SL, Burd CJ, Marshall TW, Wetherill YB, Knudsen KE (2003) Specificity of cyclin D1 for androgen receptor regulation. *Cancer Res* **63**: 4903–13
72. Ponguta LA, Gregory CW, French FS, Wilson EM (2008) Site-specific androgen receptor serine phosphorylation linked to epidermal growth factor-dependent growth of castration-recurrent prostate cancer. *J Biol Chem* **283**: 20989–1001
73. Pratt WB, Toft DO (1997) Steroid receptor interactions with heat shock protein and immunophilin chaperones. *Endocr Rev* **18**: 306–60
74. Prescott J, Coetzee GA (2006) Molecular chaperones throughout the life cycle of the androgen receptor. *Cancer Lett* **231**: 12–9
75. Rodríguez-Ubreva FJ, Cariaga-Martínez AE, Cortés MA, Romero-De Pablos M, Ropero S, López-Ruiz P, Colás B (2010) Knockdown of protein tyrosine phosphatase SHP-1 inhibits G1/S progression in prostate cancer cells through the regulation of components of the cell-cycle machinery. *Oncogene* **29**: 345–55
76. Sartor O, Pal SK (2013) Abiraterone and its place in the treatment of metastatic CRPC. *Nat Rev Clin Oncol* **10**: 6–8
77. Sato N, Sadar MD, Bruchovsky N, Saatcioglu F, Rennie PS, Sato S, Lange PH, Gleave ME (1997) Androgenic induction of prostate-specific antigen gene is repressed by protein-protein interaction between the androgen receptor and AP-1/c-Jun in the human prostate cancer cell line LNCaP. *J Biol Chem* **272**: 17485–94
78. Scher HI, Fizazi K, Saad F, Taplin ME, Sternberg CN, Miller K, de Wit R, Mulders P, Chi KN, Shore ND, Armstrong AJ, Flraig TW, Fléchon A, Mainwaring P, Fleming M, Hainsworth JD, Hirmand M, Selby B, Seely L, de Bono JS, et al (2012) Increased

- 874 survival with enzalutamide in prostate cancer after chemotherapy. *N Engl J Med*
875 **367:** 1187–97
- 876 79. Seaton A, Scullin P, Maxwell PJ, Wilson C, Pettigrew J, Gallagher R, O'Sullivan
877 JM, Johnston PG, Waugh DJJ (2008) Interleukin-8 signaling promotes androgen-
878 independent proliferation of prostate cancer cells via induction of androgen receptor
879 expression and activation. *Carcinogenesis* **29:** 1148–56
- 880 80. Sharma A, Yeow WS, Ertel A, Coleman I, Clegg N, Thangavel C, Morrissey C, Zhang
881 X, Comstock CES, Witkiewicz AK, Gomella L, Knudsen ES, Nelson PS, Knudsen
882 KE (2010) The retinoblastoma tumor suppressor controls androgen signaling and
883 human prostate cancer progression. *J Clin Invest* **120:** 4478–92
- 884 81. Sherr CJ, Roberts JM (1999) CDK inhibitors: positive and negative regulators of
885 G1-phase progression. *Genes Dev* **13:** 1501–12
- 886 82. Siegel R, Naishadham D, Jemal A (2013) Cancer statistics, 2013. *CA Cancer J Clin*
887 **63:** 11–30
- 888 83. Slamon DJ, Godolphin W, Jones LA, Holt JA, Wong SG, Keith DE, Levin WJ, Stuart
889 SG, Udove J, Ullrich A (1989) Studies of the HER-2/neu proto-oncogene in human
890 breast and ovarian cancer. *Science* **244:** 707–12
- 891 84. Sobel RE, Sadar MD (2005) Cell lines used in prostate cancer research: a com-
892 pendium of old and new lines—part 1. *J Urol* **173:** 342–59
- 893 85. Song SO, Chakrabarti A, Varner JD (2010) Ensembles of signal transduction models
894 using Pareto Optimal Ensemble Techniques (POETs). *Biotechnol J* **5:** 768–80
- 895 86. Song SO, Varner J (2009) Modeling and analysis of the molecular basis of pain in
896 sensory neurons. *PLoS One* **4:** e6758
- 897 87. Takaishi H, Konishi H, Matsuzaki H, Ono Y, Shirai Y, Saito N, Kitamura T, Ogawa
898 W, Kasuga M, Kikkawa U, Nishizuka Y (1999) Regulation of nuclear translocation of
899 forkhead transcription factor AFX by protein kinase B. *Proc Natl Acad Sci U S A* **96:**

- 900 11836–41
- 901 88. Tam L, McGlynn LM, Traynor P, Mukherjee R, Bartlett JMS, Edwards J (2007) Expression levels of the JAK/STAT pathway in the transition from hormone-sensitive to
902 hormone-refractory prostate cancer. *Br J Cancer* **97**: 378–83
- 903
- 904 89. Taneja SS, Ha S, Swenson NK, Huang HY, Lee P, Melamed J, Shapiro E, Garabedian MJ, Logan SK (2005) Cell-specific regulation of androgen receptor phosphorylation in vivo. *J Biol Chem* **280**: 40916–24
- 905
- 906 90. Tannock IF, de Wit R, Berry WR, Horti J, Pluzanska A, Chi KN, Oudard S, Théodore C, James ND, Turesson I, Rosenthal MA, Eisenberger MA, TAX 327 Investigators (2004) Docetaxel plus prednisone or mitoxantrone plus prednisone for advanced
907 prostate cancer. *N Engl J Med* **351**: 1502–12
- 908
- 909 91. Tasseeff R, Nayak S, Salim S, Kaushik P, Rizvi N, Varner JD (2010) Analysis of the
910 molecular networks in androgen dependent and independent prostate cancer revealed fragile and robust subsystems. *PLoS One* **5**: e8864
- 911
- 912 92. Tasseeff R, Nayak S, Song SO, Yen A, Varner JD (2011) Modeling and analysis of
913 retinoic acid induced differentiation of uncommitted precursor cells. *Integr Biol Camb*
914 **3**: 578–91
- 915
- 916 93. Thalmann GN, Anezinis PE, Chang SM, Zhai HE, Kim EE, Hopwood VL, Pathak S,
917 von Eschenbach AC, Chung LW (1994) Androgen-independent cancer progression
918 and bone metastasis in the LNCaP model of human prostate cancer. *Cancer Res*
919 **54**: 2577–81
- 920
- 921 94. Veeramani S, Igawa T, Yuan TC, Lin FF, Lee MS, Lin JS, Johansson SL, Lin
922 MF (2005) Expression of p66(Shc) protein correlates with proliferation of human
923 prostate cancer cells. *Oncogene* **24**: 7203–12
- 924
- 925 95. Veeramani S, Yuan TC, Chen SJ, Lin FF, Petersen JE, Shaheduzzaman S, Srivastava S, MacDonald RG, Lin MF (2005) Cellular prostatic acid phosphatase: a pro-

- tein tyrosine phosphatase involved in androgen-independent proliferation of prostate cancer. *Endocr Relat Cancer* **12**: 805–22
- 926
927
- 928 96. Villaverde AF, Banga JR (2014) Reverse engineering and identification in systems
929 biology: strategies, perspectives and challenges. *J R Soc Interface* **11**: 20130505
- 930 97. Wayman J, Varner J (2013) Biological systems modeling of metabolic and signaling
931 networks. *Curr Opin Chem Eng* **2**: 365 – 372
- 932 98. Weber MJ, Gioeli D (2004) Ras signaling in prostate cancer progression. *J Cell*
933 *Biochem* **91**: 13–25
- 934 99. Wen Y, Hu MC, Makino K, Spohn B, Bartholomeusz G, Yan DH, Hung MC (2000)
935 HER-2/neu promotes androgen-independent survival and growth of prostate cancer
936 cells through the Akt pathway. *Cancer Res* **60**: 6841–5
- 937 100. Whang YE, Armstrong AJ, Rathmell WK, Godley PA, Kim WY, Pruthi RS, Wallen
938 EM, Crane JM, Moore DT, Grigson G, Morris K, Watkins CP, George DJ (2013) A
939 phase II study of lapatinib, a dual EGFR and HER-2 tyrosine kinase inhibitor, in
940 patients with castration-resistant prostate cancer. *Urol Oncol* **31**: 82–6
- 941 101. Wilkinson MG, Millar JB (2000) Control of the eukaryotic cell cycle by MAP kinase
942 signaling pathways. *FASEB J* **14**: 2147–57
- 943 102. Xu Y, Chen SY, Ross KN, Balk SP (2006) Androgens induce prostate cancer cell pro-
944 liferation through mammalian target of rapamycin activation and post-transcriptional
945 increases in cyclin D proteins. *Cancer Res* **66**: 7783–92
- 946 103. Yamamoto A, Hashimoto Y, Kohri K, Ogata E, Kato S, Ikeda K, Nakanishi M (2000)
947 Cyclin E as a coactivator of the androgen receptor. *J Cell Biol* **150**: 873–80
- 948 104. Yeh S, Lin HK, Kang HY, Thin TH, Lin MF, Chang C (1999) From HER2/Neu signal
949 cascade to androgen receptor and its coactivators: a novel pathway by induction of
950 androgen target genes through MAP kinase in prostate cancer cells. *Proc Natl Acad
951 Sci U S A* **96**: 5458–63

- 952 105. Yeh S, Miyamoto H, Nishimura K, Kang H, Ludlow J, Hsiao P, Wang C, Su C, Chang
953 C (1998) Retinoblastoma, a tumor suppressor, is a coactivator for the androgen
954 receptor in human prostate cancer DU145 cells. *Biochem Biophys Res Commun*
955 **248**: 361–7
- 956 106. Yuan TC, Lin FF, Veeramani S, Chen SJ, Earp 3rd HS, Lin MF (2007) ErbB-2 via
957 PYK2 upregulates the adhesive ability of androgen receptor-positive human prostate
958 cancer cells. *Oncogene* **26**: 7552–9

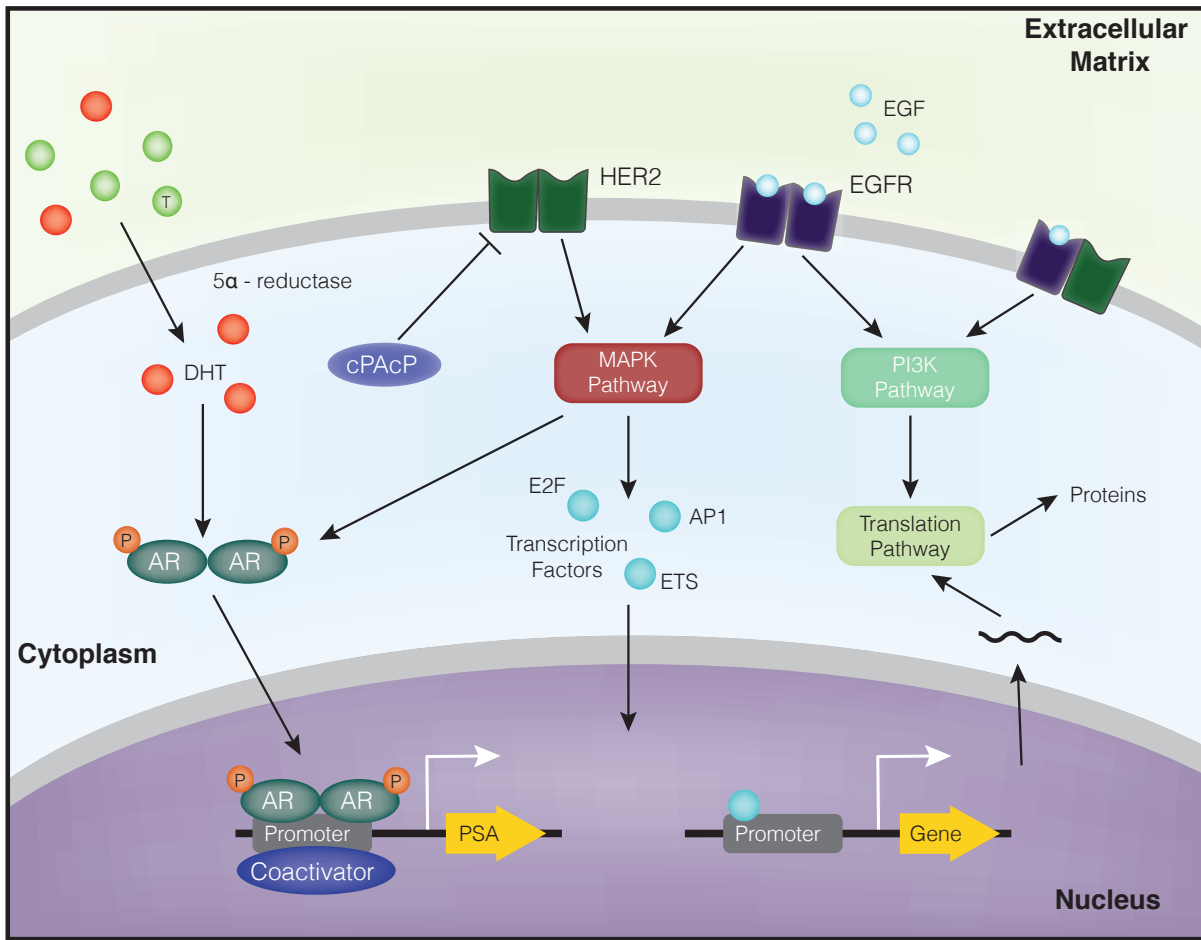


Fig. 1: Schematic overview of the prostate signaling network. The model describes hormone and growth factor induced expression of several proteins, including PSA. In the absence of outside hormones/growth factors, overactive HER2 can stimulate the MAPK and AKT pathways. AR can be activated directly by the MAPK pathway.

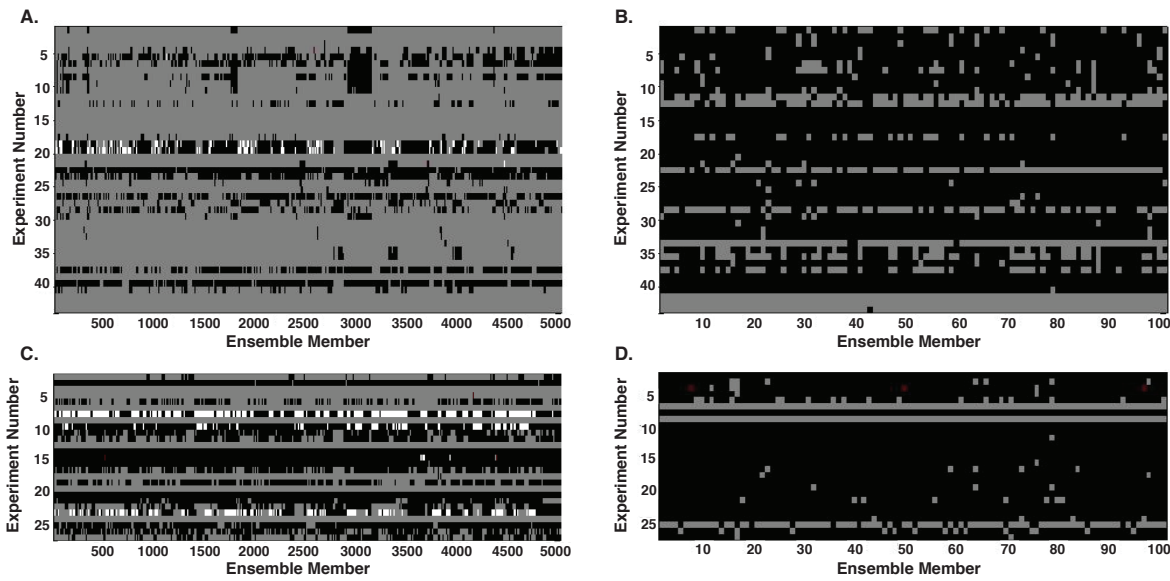


Fig. 2: Simulation results versus experimental results for training and validation data. Experiment numbers 1 through 43 were used for training, while experiments 44 through 72 were validation. Gray means the ensemble member qualitatively fit experimental data in both models. White means the ensemble member only fit the data using the new model that included HER2 heterodimerization. Red means the ensemble member fit using only the old model. Black corresponds to an incorrect cellular response in both models. A., C. Training and validation results, respectively, for entire ensemble population using both the original model and an updated model including HER2 heterodimerization ($N = 5000$). B., D. Simulation results for training and validation of a random set of 100 members using both models.

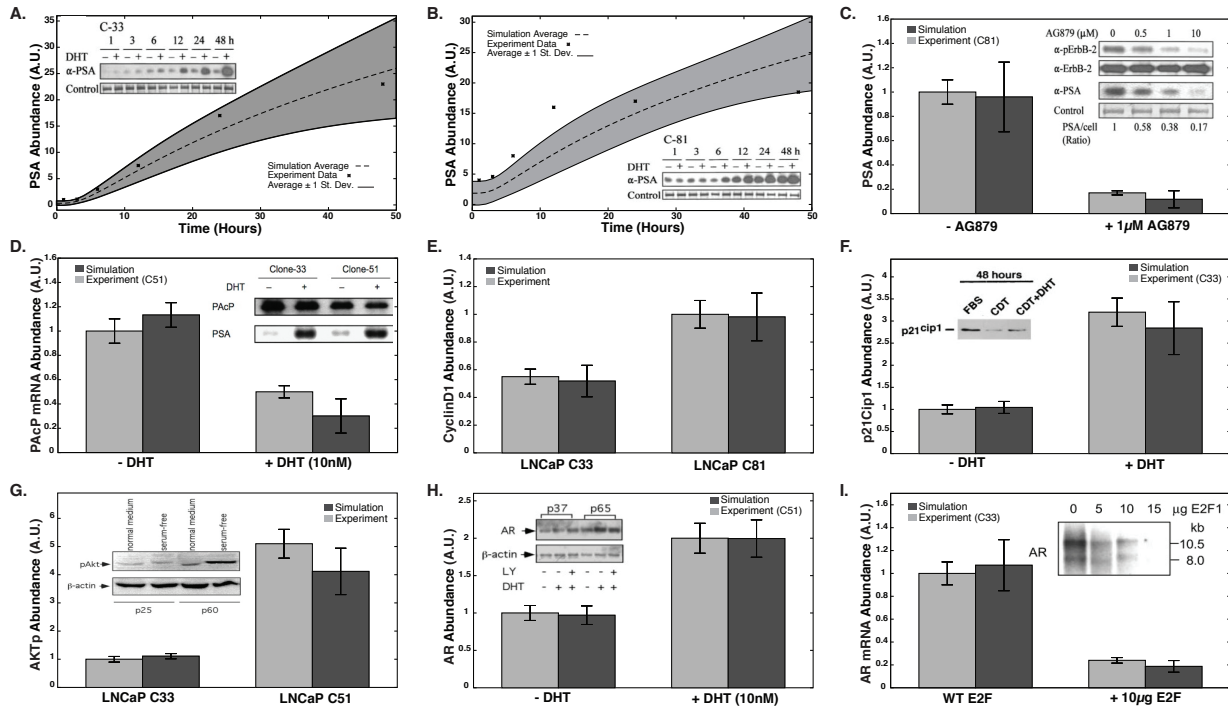


Fig. 3: Ensemble performance against selected training objectives ($N = 5000$). A, B. Time course data for PSA concentration due to a stimulus of 10 nM DHT in LNCaP C33 cells and LNCaP C81 cells, respectively (O2, O3). C. PSA levels in the presence and absence of a HER2 inhibitor (LNCaP C81 cells, O7). D. PAcP mRNA levels at 72 hours in the presence and absence of DHT (LNCaP C51 cells, O14). E. Steady-state cyclin D levels in LNCaP C33 vs. C81 (O17). F. p21Cip1 levels at 48 hrs in the presence and absence of DHT (LNCaP C33, O25). G. Steady-state AKT phosphorylation levels in LNCaP C33 vs. C51 (O30). H. AR levels at 24 hours in the presence and absence of DHT (LNCaP C51, O31). I. AR mRNA levels in the presence and absence of E2F over expression (LNCaP C33, O34). Error bars denote plus and minus one standard deviation above the mean.

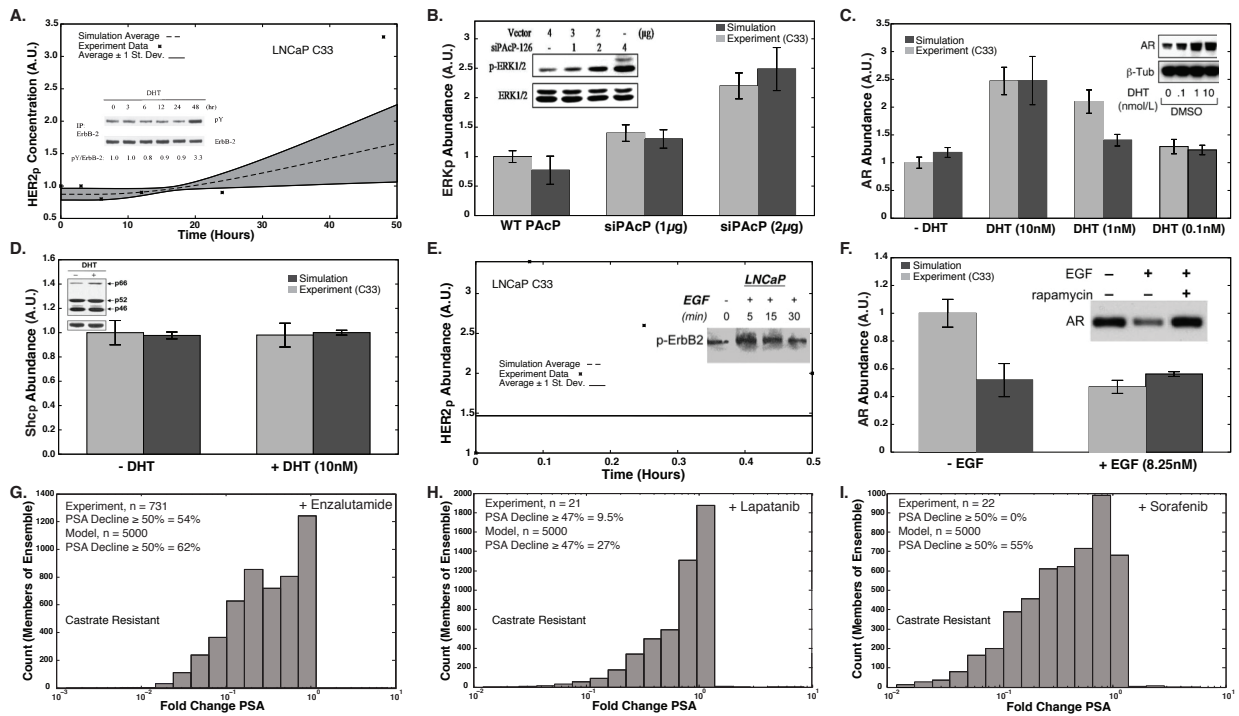


Fig. 4: Blind model predictions for the ensemble ($N = 5000$). The model ensemble's predictive ability was assessed by comparing simulation versus experimental data not used for training. A. Time course data for HER2 phosphorylation due to a stimulus of 10 nM DHT (LNCaP C33, P1). B. ERK phosphorylation levels in the presence and absence of a PAcP inhibitor (LNCaP C33 cells, P3). C. AR levels at 24 hrs in varying levels of DHT (LNCaP C33, P17). D. Shc phosphorylation levels at 24 hrs in the presence and absence of DHT (LNCaP C33, P22). E. Time course data for HER2 phosphorylation due to a stimulus of 1.6 nM EGF (LNCaP C33, P7). F. AR levels in varying levels of EGF (LNCaP C33, P14). G, H, I. Fold change in PSA concentration due to drug stimulus: enzalutamide, lapatinib, and sorafenib. Error bars denote plus and minus one standard deviation above the mean.

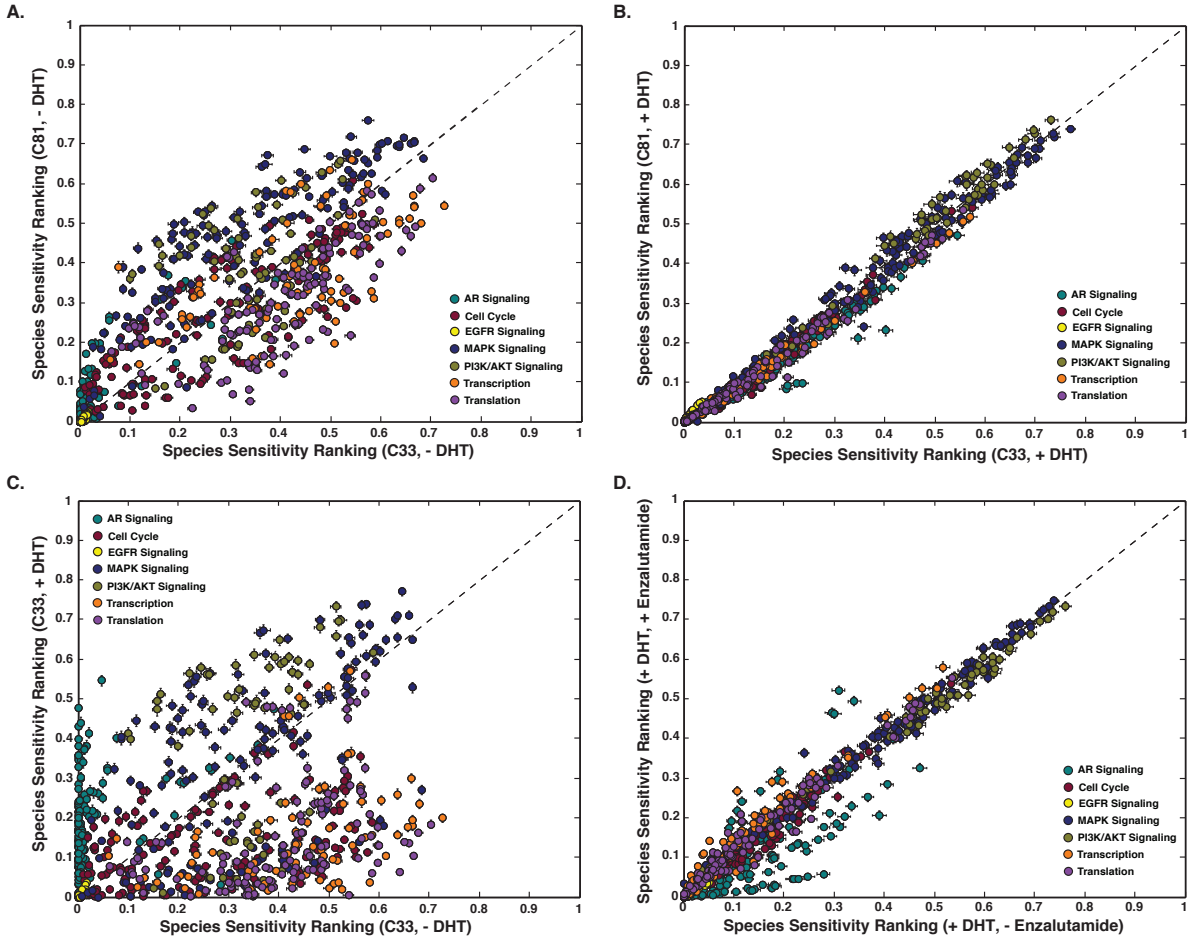


Fig. 5: Sensitivity analysis of a population of prostate models ($N = 500$). Species with a low sensitivity are considered robust, while species with a high sensitivity ranking are considered fragile. **A, B.** Sensitivity ranking of network species in AD versus CR cells in the absence (presence) of DHT. **C.** Sensitivity ranking of network species in AD cells in the absence and presence of DHT. **D.** Sensitivity ranking of network species in CR cells in the presence and absence of enzalutamide with a DHT stimulus. Error bars denote standard error with $N = 500$.

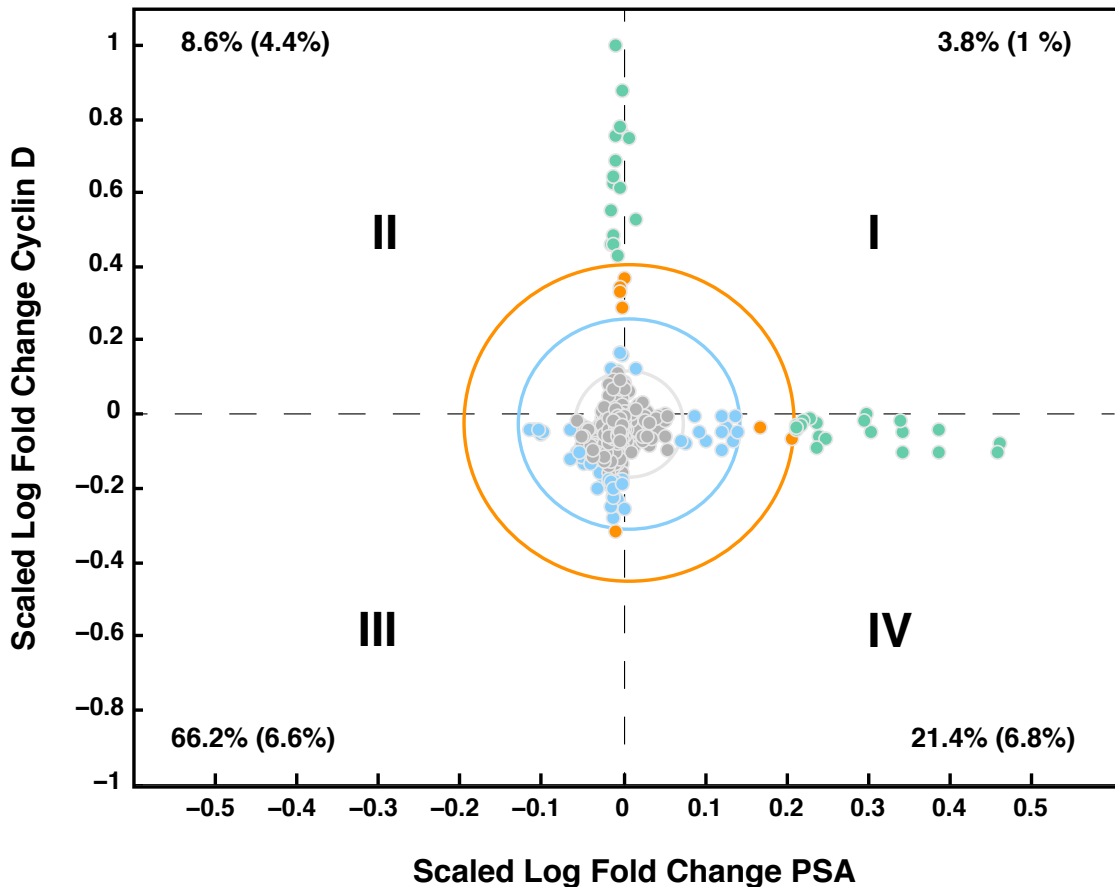


Fig. 6: Robustness analysis of a population of CR prostate models with Raf knock-out ($N = 500$). A log fold change of greater than zero implies that the concentration of the protein increased with the knock-out of Raf, while a log fold change of less than zero indicates that the concentration of protein decreased. A log of fold change equal to 0, shows no response due to Raf knock-out. Three distinct regions emerge in Raf knock-out case: (1) PSA increases, (2) cyclin D concentration increases, and (3) PSA and cyclin D concentration decrease.

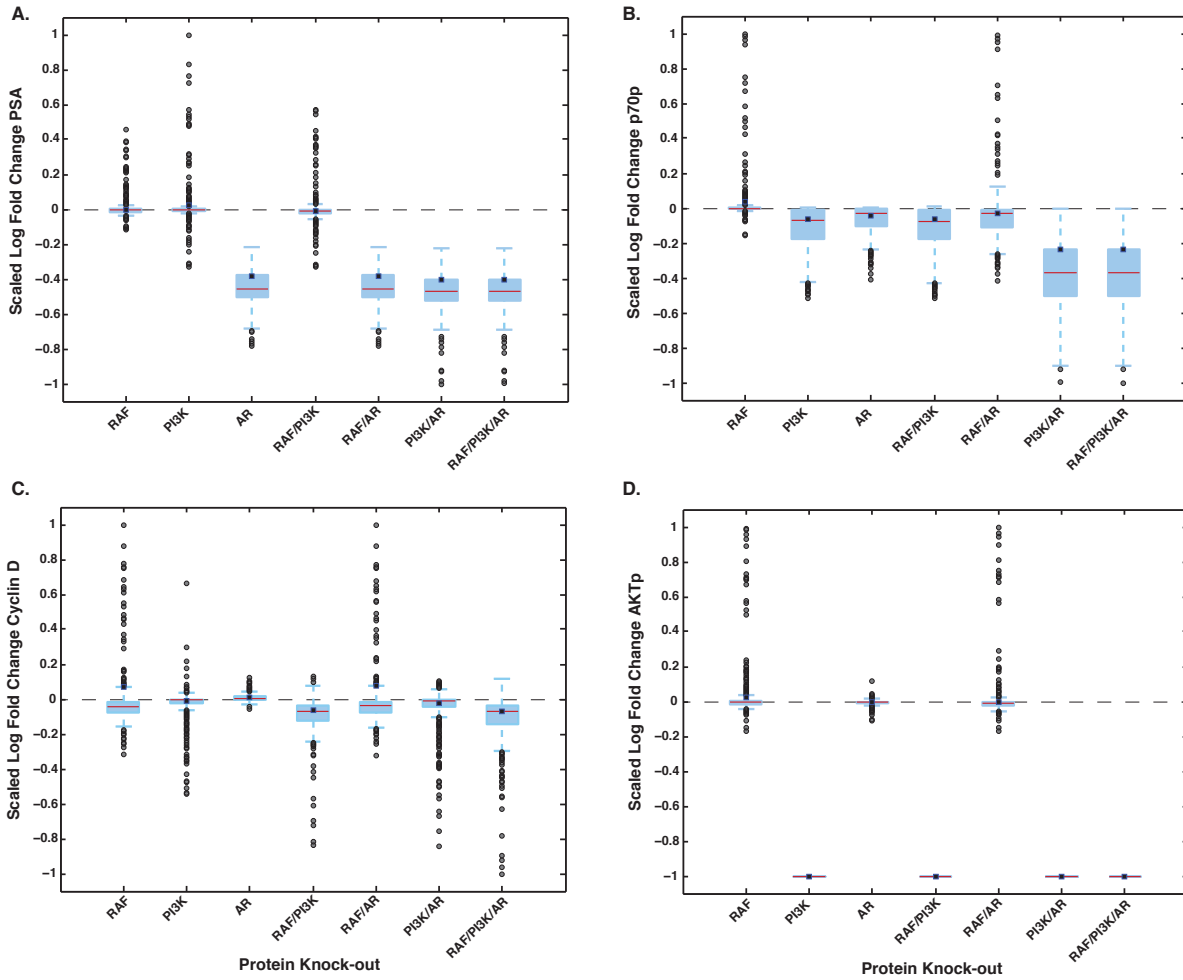


Fig. 7: Robustness analysis of a population of CR prostate models with seven protein knock-out cases ($N = 500$). A log fold change of greater than zero implies that the concentration of the protein increased with the knock-out, while a log fold change of less than zero indicates that the concentration of protein decreased. A log of fold change equal to 0, shows no response due to the knock-out. A.,B.,C.,D. Log robustness of PSA, p70p, Cyclin D, and AKTp versus protein knock-out. A CR LNCaP cell was assumed for all knock-out cases.

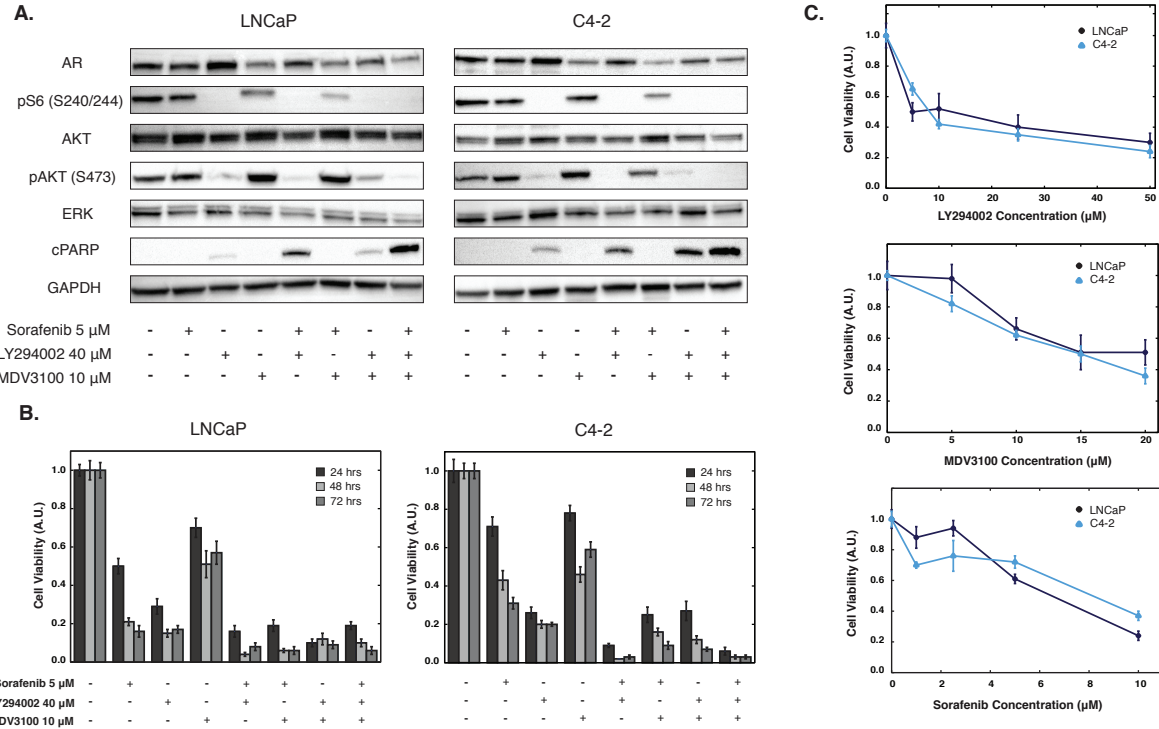


Fig. 8: Experimental results for multiple drug combinations on two prostate cancer cell lines, LNCaP and C4-2. A. Western blot analysis of AR, pS6, AKT, pAKT, ERK and cleaved PARP in LNCaP and C4-2 cell lines treated for 24 hrs with DMSO (control), sorafenib (5 μ M), LY294002 (40 μ M), and MDV3100 (10 μ M) alone or in combination (at least 3 repeats). B. Cells (LNCaP and C4-2) were treated for 24, 48 and 72 hrs with sorafenib (5 μ M), LY294002 (40 μ M), and MDV3100 (10 μ M) and cell viability was measured using MTT Assay. Values were normalized to DMSO (control). C. Cell viability results for LNCaP and C4-2 cells at varying concentration of sorafenib, LY294002, and MDV3100 after 24 hrs of treatment. Values were normalized to DMSO (control). Error bars represent standard error (at least 3 repeats with triplicates performed in each experiment).

959 **Supplementary materials**

960 **Estimation of a population of models using Pareto Optimal Ensemble Techniques**

961 **(POETs).** We used multiobjective optimization to estimate an ensemble of prostate mod-
962 els. Although computationally more complex than single-objective formulations, multiob-
963 jective optimization can be used to address qualitative conflicts in training data arising
964 from experimental error or cell-line artifacts [34]. In this study we used the Pareto Optimal
965 Ensemble Technique (POETs) to perform the optimization. POETs integrates standard
966 search strategies, e.g., Simulated Annealing (SA) or Local Pattern Search (PS) with a
967 Pareto-rank fitness assignment [85]. The mean squared error, η_j , of parameter set \mathbf{k} for
968 training objective j was defined as:

$$\eta_j(\mathbf{p}_k) = \frac{1}{N} \sum_i^N \frac{(\hat{x}_{i,j} - \beta_j x(\mathbf{p}_k)_{i,j})^2}{\hat{\sigma}_{i,j}^2} \quad (\text{S1})$$

969 The symbol $\hat{x}_{i,j}$ denotes scaled experimental observations (from training objective j) while
970 $x(\mathbf{p}_k)_{i,j}$ denotes the simulation output (from training objective j). The quantity i denotes
971 the sampled time-index or condition, and N denotes the number of time points or condi-
972 tions for experiment j . The standard deviation, $\hat{\sigma}_{i,j}$, was assumed to be equal to 10% of the
973 reported observation, if no experimental error was reported. β_j is a scaling factor which
974 is required when considering experimental data that is accurate only to a multiplicative
975 constant. In this study, the experimental data used for training and validation was typi-
976 cally band intensity from immunoblots, where intensity was estimated using the ImageJ
977 software package [1]. The scaling factor used was chosen to minimize the normalized
978 squared error [5]:

$$\beta_j = \frac{\sum_i (\hat{x}_{i,j} x_{i,j} / \hat{\sigma}_{i,j}^2)}{\sum_i (x_{i,j} / \hat{\sigma}_{i,j})^2} \quad (\text{S2})$$

979 By using the scaling factor, the concentration units on simulation results were arbitrary,
 980 which was consistent with the arbitrary units on the experimental training data. All simu-
 981 lation data was scaled by the corresponding β_j .

982 We computed the Pareto rank of parameter set \mathbf{k}_{i+1} by comparing the simulation error
 983 at iteration $i + 1$ against the simulation archive, denoted as \mathbf{K}_i . We used the Fonseca and
 984 Fleming ranking scheme [23] to estimate the rank of the parameter set \mathbf{k}_{i+1} . Parameter
 985 sets with increasing rank are progressively further away from the optimal trade-off surface.
 986 The parameter set \mathbf{k}_{i+1} was accepted or rejected by the SA with probability $\mathcal{P}(\mathbf{k}_{i+1})$:

$$\mathcal{P}(\mathbf{k}_{i+1}) \equiv \exp \{-\text{rank}(\mathbf{k}_{i+1} | \mathbf{K}_i) / T\} \quad (\text{S3})$$

987 where T is the computational annealing temperature. The Pareto rank for \mathbf{k}_{i+1} is denoted
 988 by $\text{rank}(\mathbf{k}_{i+1} | \mathbf{K}_i)$. The annealing temperature was adjusted according to the schedule
 989 $T_k = \beta^k T_0$ where β was defined as $\beta = \left(\frac{T_f}{T_o}\right)^{1/10}$. The initial temperature was given by
 990 $T_0 = n/\log(2)$, with $n = 4$ and the final temperature $T_f = 0.1$ used in this study. The
 991 epoch-counter k was incremented after the addition of 50 members to the ensemble. As
 992 the ensemble grew, the likelihood of accepting a high rank set decreased. Parameter sets
 993 were generated by applying a random perturbation in log space:

$$\log \mathbf{k}_{i+1} = \log \mathbf{k}_i + \mathcal{N}(0, \nu) \quad (\text{S4})$$

994 where $\mathcal{N}(0, \nu)$ is a normally distributed random number with zero mean and variance ν ,
 995 set as 0.1 in this model. The perturbation was applied in log space to account for large
 996 variation in parameter scales and to ensure positive parameter values. We used a local
 997 pattern search every q steps, in our case 20, to minimize error for a single randomly se-
 998 lected objective. The local pattern-search algorithm used has been described previously
 999 [24].

Table T1: Objective function list along with species measured, stimulus, cell-type, steady state (SS) vs dynamic (D) and the corresponding literature reference.

	O#	Species	Cell Type	Stimulus	SS or D	Source
1000	O1	PSA	C33/C81	0	SS	[50]
	O2	PSA	C33	DHT	D	[50]
	O3	PSA	C81	DHT	D	[50]
	O4	ERK-p	C33	DHT	D	[50]
	O5	ERK-p	C81	DHT	D	[50]
	O6	PSA	C33	HER2 Knockdown	SS	[50]
	O7	PSA	C81	HER2 Knockdown	SS	[50]
	O8	PSA	C33	MEK Up	SS	[50]
	O9	PSA	C81	MEK Down	SS	[50]
	O10	PSA	C33	HER2 Up	SS	[50]
	O11	ERK-p	C33	HER2 Up	SS	[50]
	O12	AR	C33/C51/C81	0	SS	[55]
	O13	PAcP mRNA	C33	DHT	D	[55]
	O14	PAcP mRNA	C51	DHT	D	[55]
	O15	PAcP mRNA	C81	DHT	D	[55]
	O16	HER2-p	C33/C51/C81	0	SS	[106]
	O17	Cyclin D	C33/C81	0	SS	CITE
	O18	Cyclin D	C33	EGF	D	[70]
	O19	Cyclin D mRNA	C33	EGF	D	[70]
	O20	AKT-p	C51/LNCaP-Rf	0	SS	[66]
	O21	p27Kip1	C51/LNCaP-Rf	0	SS	[66]
	O22	p21Cip1	C51/LNCaP-Rf	0	SS	[66]
	O23	Rb-p	C33	DHT	D	[102]
	O24	p70-p	C33	DHT	D	[102]
	O25	p21Cip1	C33	DHT	D	[47]
	O26	p27Kip1	C33	DHT	D	[47]
	O27	PSA mRNA	C33	Cyclin E Up + DHT	D	[103]
	O28	AR mRNA	C33	Cyclin E Up + DHT	D	[103]
	O29	PSA mRNA	C33	HER2 Up	SS	[104]
	O30	AKT-p	C33/C51	0	SS	[53]
	O31	AR	C51	DHT	D	[53]

1002	O32	AR	C33	DHT	D	[12]
	O33	Cyclin D1b mRNA	C33	Sam68 Knockdown	SS	[69]
	O34	AR mRNA	C33	E2F Up	SS	[18]
	O35	AR	C33	E2F Up	SS	[18]
	O36	AR Cyclin E	C33	E2F Up	SS	[18]
	O37	PSA	C33	E2F Up	SS	[18]
	O38	cPAcP	C33	DHT	D	[63]
	O39	Cyclin D	C33	DHT	D	[102]
	O40	4EBP1-p	C33	DHT	D	[102]
	O41*	PAcP mRNA	C33/C51/C81	0	SS	[55]
	O42*	p16INK4	C51/C81	0	SS	[66]
	O43*	cPAcP	C33/C51/C81	0	SS	[56]

1003 **Table T2:** Blind Prediction list along with species measured, stimulus, cell-type, steady state (SS) vs dynamic (D) and the corresponding literature reference.

Prediction#	Species	Cell Type	Stimulus	SS or D	Source
1004	P1	HER2-p	C33	DHT	D [63]
	P2	p27Kip1	C33	SHP Knockdown	D [75]
	P3	ERK-p	C33	PAcP Knockdown	SS [14]
	P4	AKT-p	C33	PAcP Knockdown	SS [14]
	P5	Cyclin D1	C33	PAcP Knockdown	SS [14]
	P6	EGFR-p	C33	EGF	D [11]
	P7	HER2-p	C33	EGF	D [11]
	P8	EGFR-p	LNCaP-AI	EGF	D [11]
	P9	HER2-p	LNCaP-AI	EGF	D [11]
	P10	CyclinE	C33	DHT	D [47]
	P11	CDK2	C33	DHT	D [47]
	P12	HER2-p	C33/C81	0	SS [14]
	P13	AR	C33	EGF	D [8]
	P14	AR	C33	EGF	D [15]
	P15	p27Kip1	C33	DHT	D [21]
	P16	Rb-p	C33	DHT	D [47]
	P17	AR	C33	DHT	D [8]
	P18	AKT-p	C33	DHT	D [8]
	P19	PSA	C33	EGF + DHT	D [8]
	P20	PSA	C33	EGF	D [8]
	P21	Cyclin D1	C33	Sam68 Knockdown	SS [7]
	P22	Shc	C33	DHT	D [94]
	P23	Shc	C33	EGF	D [94]
	P24	Shc	C33/C81	0	SS [94]
	P25	AR	C33	AKT-p Knockdown	SS [32]
	P26	AR	LNCaP AI	AKT-p Knockdown	SS [32]
	P27	4EBP1 bound eIF4E	C33/LNAI	0	SS [27]
	P28	Shc-p	C33/C51/C81	0	SS [49]
	P29	Shc-p	C33	EGF	D [49]
	P30	PSA Response	CRPC Patients	enzalutamide	D [78]
	P31	PSA Response	CRPC Patients	sorafenib	D [17]

1005

P32	PSA Response	CRPC Patients	lapatinib	D	[100]
P33	PSA Response	ADPC Patients	lapatinib	D	[58]

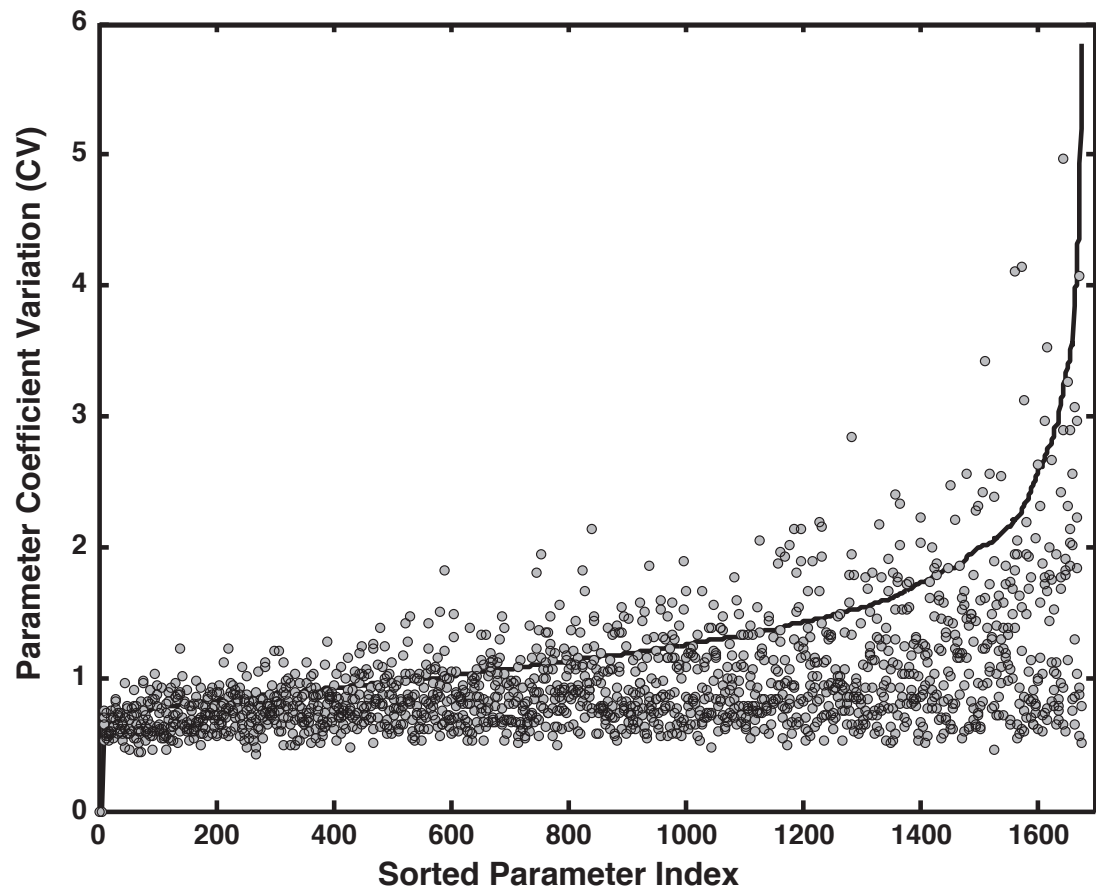


Fig. S1: Coefficient of variation (CV) of model parameters estimated using POETs. The solid line denotes the mean CV calculated over the entire ensemble ($N = 5000$). The points denote the mean CV of the 500 ensemble members used for sensitivity and robustness calculations. Over the ensemble, the coefficient of variation (CV) of the kinetic parameters spanned 0.59 - 5.8, with 33% of the parameters having a CV of less than one.

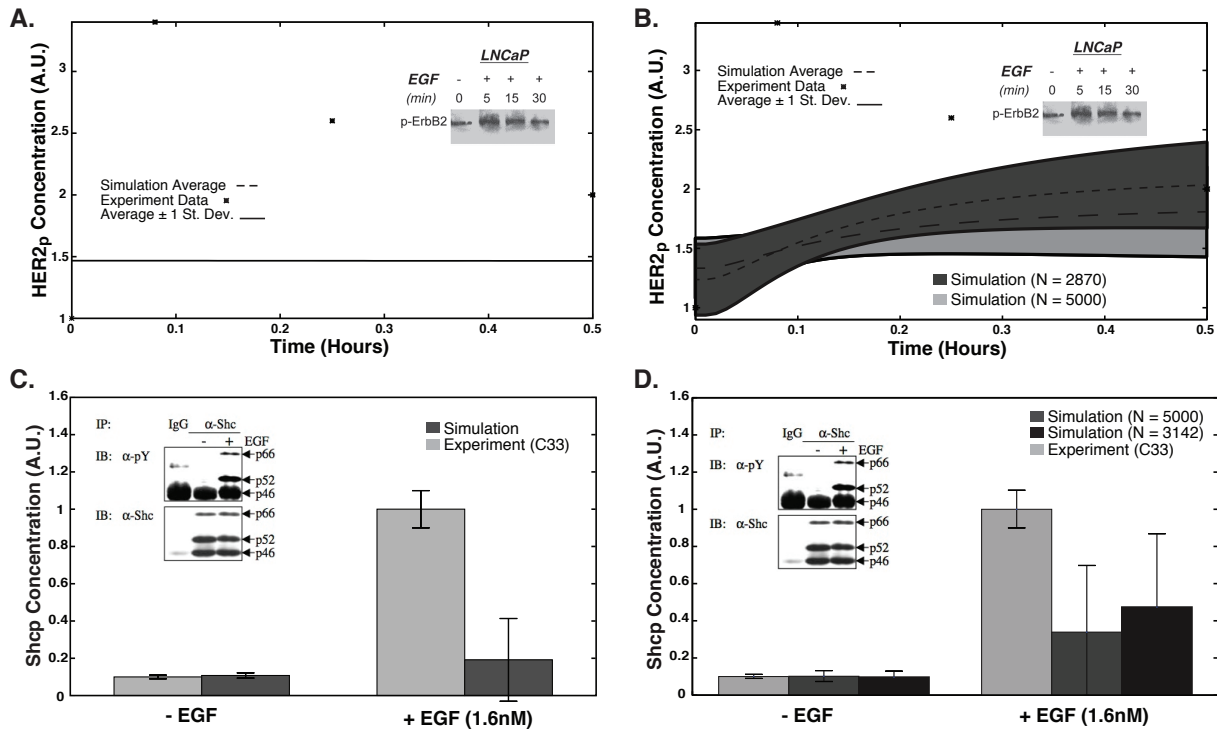


Fig. S2: Blind model predictions for the ensemble with the original and updated model (EGFR and HER2 heterodimer). A,B. Time course data for HER2 phosphorylation due to a stimulus of 1.6 nM EGF (LNCaP C33, P7) for the old and new model, respectively. Dark grey shows only parameters improved by the updated model (N=2870) while light grey show all parameter sets (N=5000). C,D. Shc phosphorylation levels at 16 hrs in the presence and absence of 1.6 nM EGF (LNCaP C33, P29) for the old and new model, respectively. Light grey denotes experimental data, mid grey denotes simulation results for all parameters (N=5000), and black denotes only parameters improved by the updated model (N=3142). Error bars denote plus and minus one standard deviation above the mean.

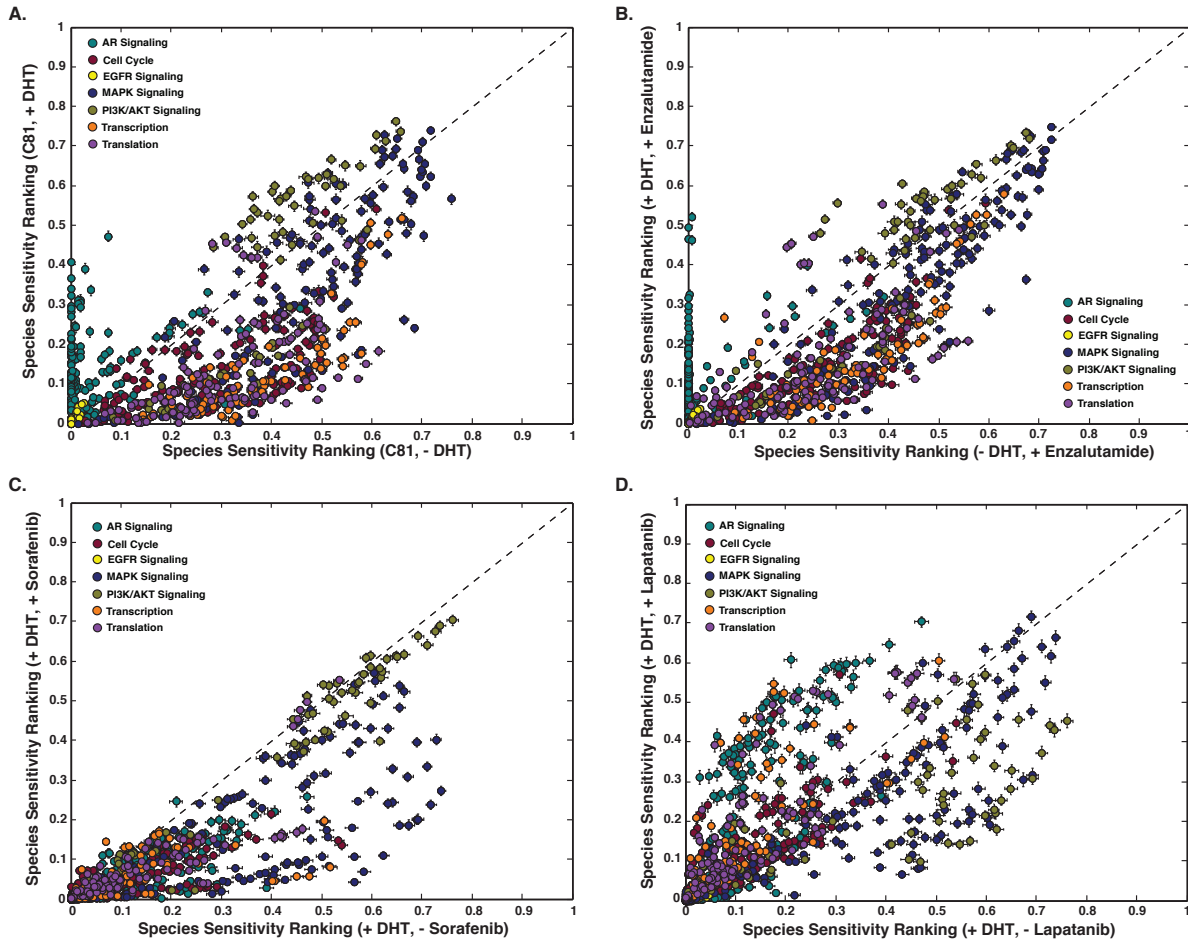


Fig. S3: Sensitivity analysis of a population of prostate models ($N = 500$). Species with a low sensitivity are considered robust, while species with a high sensitivity ranking are considered fragile. A Sensitivity ranking of network species in CR cells in the absence and presence of DHT. B. Sensitivity ranking of network species in CR cells in the presence of enzalutamide in the presence and absence of a DHT stimulus. C., D. Sensitivity ranking of network species in CR cells in the presence and absence of sorafenib and lapatinib, respectively, with a DHT stimulus. Error bars denote standard error with $N = 500$.

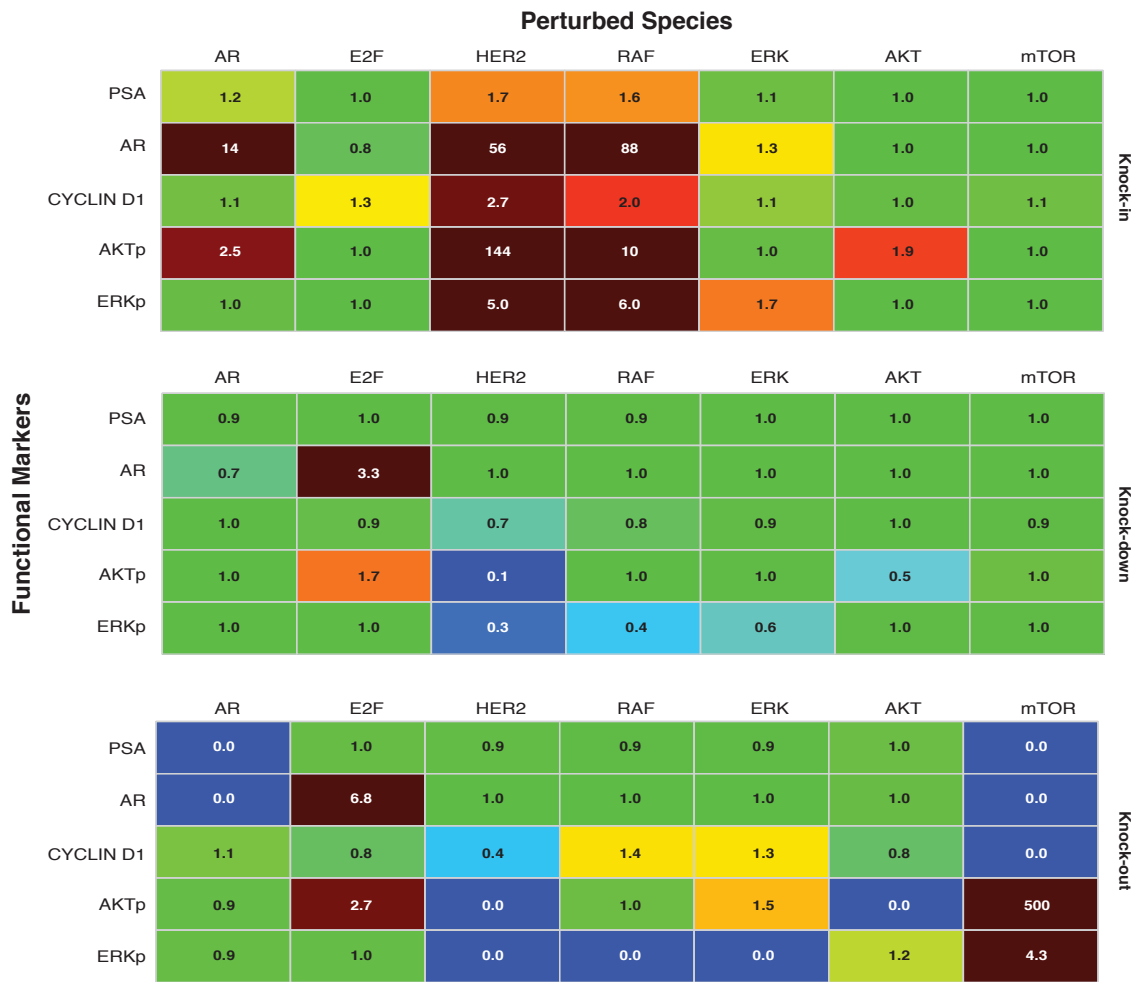


Fig. S4: Robustness analysis of protein markers. Expression level of key proteins was altered by a factor of 2, 0.1, or 0 (knock-in, knock-down, or knock-out) and robustness coefficients were calculated for five key protein markers. Simulations shown were from CR cells, with indicated perturbation. Mean of 500 ensemble members is shown.

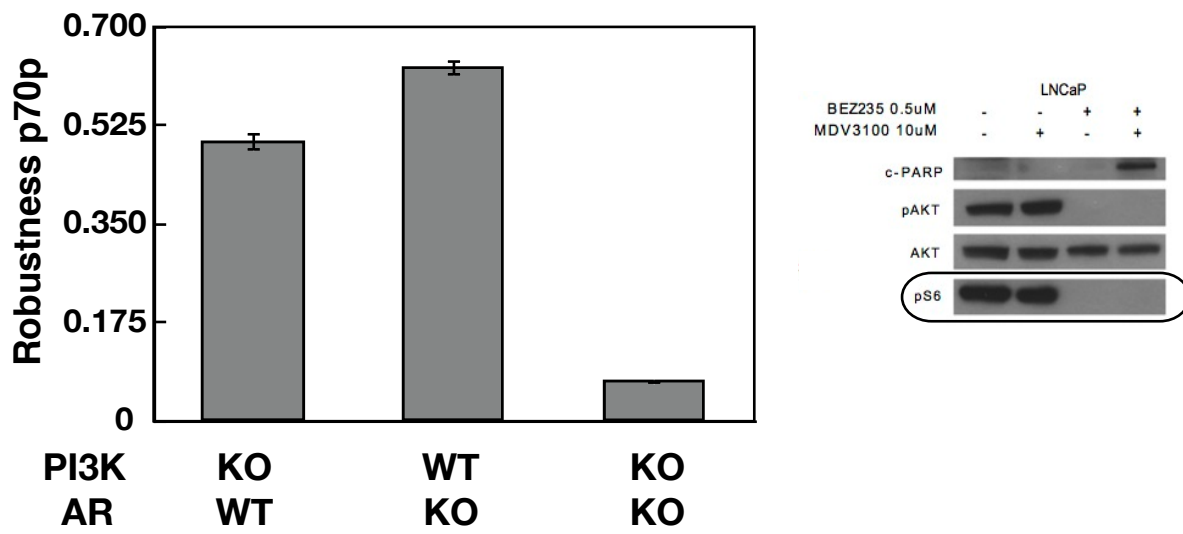


Fig. S5: Dual knock-out of AR and PI3K leads to decreased expression of activated p70. A., B, C. Robustness coefficient of activated p70 (S6) in the PI3K knock-out, AR knock-out, and dual knock-out cases, respectively. The control was the basil CR LNCaP wild type case. Error bars denote plus and minus one standard error above the mean with N = 500. Experimental data is from Carver, et al [10].